LASER INTERFEROMETER GRAVITATIONAL WAVE OBSERVATORY
- LIGO -
==========
LIGO SCIENTIFIC COLLABORATION

Technical Note	**LIGO-T1200031–v3**	2012/05/15

Report of the 3rd Generation LIGO Detector Strawman Workshop

R. Adhikari, K. Arai, S. Ballmer, E. Gustafson, S. Hild

Distribution of this document:
LIGO Scientific Collaboration

California Institute of Technology
LIGO Project, MS 18-34
Pasadena, CA 91125
Phone (626) 395-2129
Fax (626) 304-9834
E-mail: info@ligo.caltech.edu

Massachusetts Institute of Technology
LIGO Project, Room NW22-295
Cambridge, MA 02139
Phone (617) 253-4824
Fax (617) 253-7014
E-mail: info@ligo.mit.edu

LIGO Hanford Observatory
Route 10, Mile Marker 2
Richland, WA 99352
Phone (509) 372-8106
Fax (509) 372-8137
E-mail: info@ligo.caltech.edu

LIGO Livingston Observatory
19100 LIGO Lane
Livingston, LA 70754
Phone (225) 686-3100
Fax (225) 686-7189
E-mail: info@ligo.caltech.edu

http://www.ligo.org/

Contents

1 Introduction

A strong scientific case can be made for improving upon the sensitivity of the second generation detectors (aLIGO, AdVirgo, KAGRA). R & D over the last decade indicates that it should be possible to make a factor of 3-5 improvement.

From January 9-12, 2012 the LIGO Scientific Collaboration (LSC) Instrument Science Working Groups held a workshop to begin studying designs for third generation interferometers to be installed at the existing LIGO sites.

The following pointer provides information about this first Strawman Workshop https://nodus.ligo.caltech.edu:30889/wiki/doku.php?id=strawman

The purpose of this workshop was to compare the sensitivity of a few different designss. These Strawman Designs came from three teams (Red, Green and Blue) in an attempt to explore all "reasonable" design space and to create a basis for comparing different design ideas. The Red Team was lead by Stefan Hild, the Green Team by Stefan Ballmer and the Blue Team by Rana Adhikari.

Discussions were held to begin to understand the scope of the research and development effort required to implement each of the different designs. The Green team decided to continue work on their designs before presenting a representative sensitivity curve. For the remainder of this first report we will concentrate on the Red and Blue designs but expect to add sections on the Green Design in future Strawman Meeting Reports.

This work is not a technical down select for a next generation interferometer. This is an excercise to start working towards a conceptual design. As described throughout this document, a great deal of analysis and experimentation is required before we know enough to choose between the various possible designs.

In Sections 2 and 3 we describe the Red and Blue designs. In Section 5 we compare and contrast the two designs. Discussions of the Research and Develpment required to implement each of these designs are contained in Section 6.

We begin with the estimated sensitivity curves for LIGO, VIRGO, aLIGO, Advanced VIRGO, LCGT, a LIGO and the Einstein Telescope in Figure 1 .

The LSC Instrument Science White Paper [1] also covers many of these issues.

1. phased integration or shutdown for long time (2-3 years)
2. quant evaluation of IFO upgrades
3. add graphic of a couple of timeline possibilities - include India, ET, DECIGO

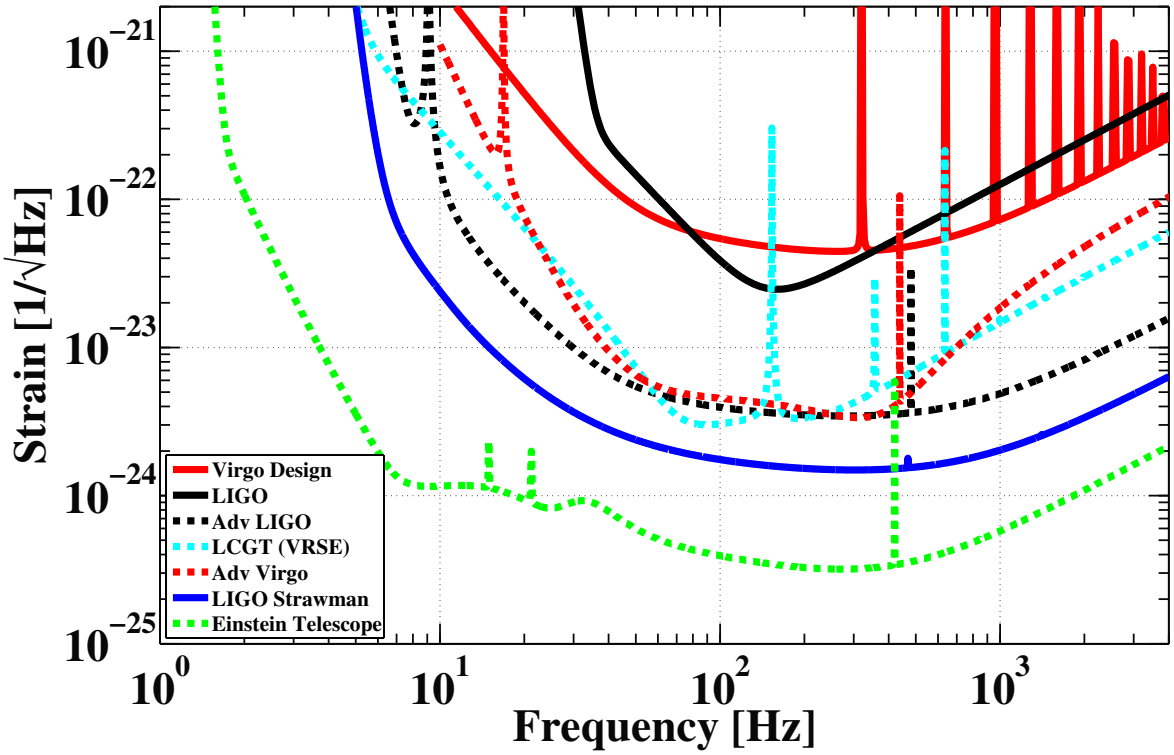

Figure 1: Comparison of ground based detectors' design curves. replace Strawman w/ R and B curves

2 Red Team Design

This section gives an overview of the LIGO-3 Strawman design of Team Red. In section 2.1 we give a brief outline of the assumptions and boundaries that were used as a starting point for the Red Team Design. A summary of the Team Red sensitivity and the parameters that were used to calculate it are then given in section 2.2.

A detailed description of the Team Red design (including all relevant noise calculations, a discussion of the required R+D and a rough estimate of the corresponding hardware cost per interferometer), can be found in LIGO-T1200005-v2[1]. The Red Team Design sensitivity data can be downloaded from LIGO-T1200047-v1[2].

2.1 Working Assumptions Used by Team Red

Our considerations are based on three input parameters that had initially (Nov 2011) been agreed on between the Straw man team leaders:

- The cost of the Advanced LIGO upgrade program was assumed to be limited to a maximum range of 50 to 100 million USD for all interferometers together.
- Regarding the anticipated timeline we assumed that all technologies included in our design should be mature enough to be compatible with an installation in 2018, assuming we start now with the required R&D and carry out the required prototyping over the next 5 years.
- Due to the current lack of practical experience with compensation of thermal lensing effects in the few hundred kilowatt range, we also assumed that the Advanced LIGO upgrades will initially not use any higher circulating light power as in the Advanced LIGO baseline (800 kW in the arm cavities).

Based on these input parameters the Red Team developed the following working assumptions on which the red design is based:

- From the previous point one can deduce, that the considered upgrades have to use to a large extend the same vacuum infrastructure as Advanced LIGO. Therefore we assumed that moderate changes of the vacuum system in the central and end stations will be possible, but assumed that no changes to the 4 km long vacuum tubes are possible.
- In addition we assumed that the seismic pre-isolation system is off limits, as replacing it would probably not fit within the targeted budget.
- Another assumption we made was to keep the test masses and their suspensions at room temperature.

[1] https://dcc.ligo.org/cgi-bin/private/DocDB/ShowDocument?docid=78100
[2] https://dcc.ligo.org/cgi-bin/private/DocDB/ShowDocument?docid=86562

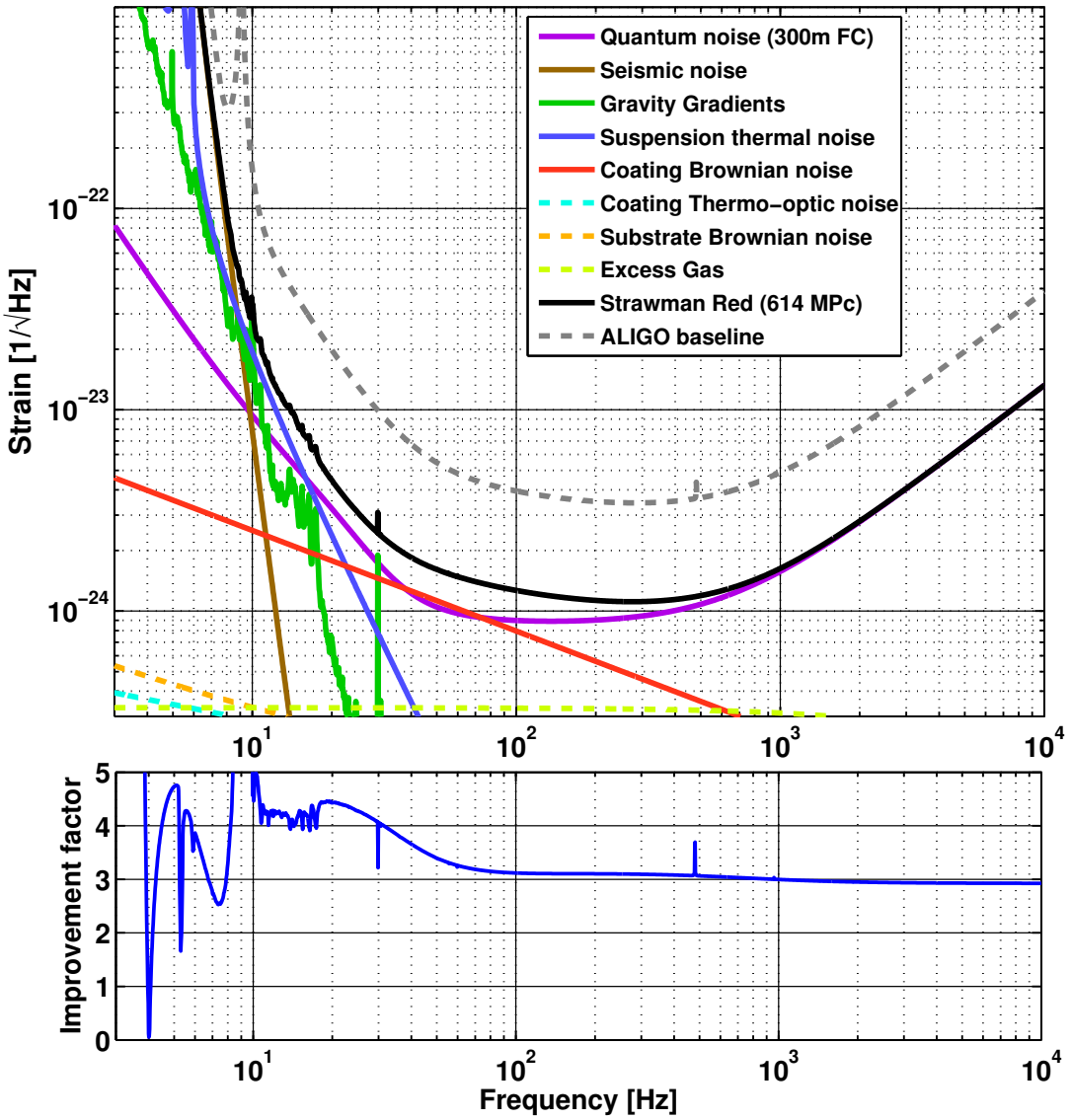

Figure 2: Noise budget for the LIGO-3 Strawman Red design (upper subplot) and the linear improvement factor compared to Advanced LIGO (lower subplot). The key parameters used to calculate this sensitivity curve can be found in Table shown in Table 1.

Due to the limited time frame available for the strawman excerise so far (Nov 2011 to Jan 2012) we focussed our efforts nearly entirely on evaluating the 'fundamental' noise sources and in most cases did not consider implications on technical noise sources, such as control noise etc. Moreover, since at the current stage our focus was set on identifying useful technologies for advanced LIGO upgrades, so far we did not perform any detailed parameter optimisation (on the percent level), to 'squeeze' the last few Mpc of binary neutron star inspiral range out of Strawman Red.

Please note that the above stated input parameters might change in future and other time scales, or financial frames will be considered to be more realistic. In that case the Strawman Red design might need to adjusted correspondingly.

2.2 Red Team Sensitivity

The full Strawman Red noise budget and the corresponding sensitivity described in this section is shown in Figure 2. The key parameters used for the calculation of this sensitivity are shown in Table 1. In the following list we give a brief overview of the assumed changes, while a more detailed description for each fundamental noise source can be found in LIGO-T1200005-v2:

- **Suspension Thermal Noise:** We assumed fused silica suspensions at room temperature, with the length of the last stage being increased from 0.6 to 1.2 m. In addition the weight of the test mass was increased to 160 kg and the fibre geometry was accordingly adapted. These changes provide a suspension thermal noise reduction of about a factor 3 to 4 above 10 Hz.

- **Seismic Noise:** The increased length of the last suspension stage also improves the seismic noise by a factor 2. No subtraction techniques have been included.

- **Newtonian Noise:** We based our calculations on measured seismic data from LLO ETMX. We assumed a seismic level corresponding to the 90th percentile and a subtraction factor of 5. This turns out to be roughly equivalent to the 10th percentile without any subtraction.

- **Coating Thermal Noise:** We assumed an overall reduction of coating noise by a factor 3.2. Increasing the beam size by a factor 1.6 reduces the coating noise by a factor 1.6. In addition we assumed a further reduction of a factor 2 which can come from improved coatings or the application of Kahlili cavities or the use of waveguide mirrors or the application of alternative beam shapes.

- **Gas Noise:** Increasing the beam size on the test masses slightly reduces the gas noise.

- **Quantum noise:** We assumed the same interferometer configuration and optical power as for aLIGO. The quantum noise improvements originate from an increased test mass weight of 160 kg and the injection of frequency dependent squeezed light. We consider an initial squeezing level of 20 dB and losses of 9 % plus the roundtrip loss in the filter cavity. The filter cavity has a length of 300 m and a roundtrip loss of 30 ppm.

Strawman Red Design Overview		
Subsystem and Parameters	**Advanced LIGO Baseline Design**	**Strawman Red Design**
Sensitivity		
Binary Neutron Star Inspiral Range	200 Mpc	614 Mpc
Anticipated Strain Sensitivity	$3.5 \cdot 10^{-24}/\sqrt{\text{Hz}}$ @ 300 Hz	$1.2 \cdot 10^{-24}/\sqrt{\text{Hz}}$ @ 250 Hz
Instrument Topology		
Interferometer	Dual-recycled Michelson with Armcavities	Dual-recycled Michelson with Armcavities
Quantum Noise Reduction	n.a	Frequency-dependent input squeezing
Laser and Optical Parameters		
Laser Wavelength	1064 nm	1064 nm
Optical Power at Test Masses	730 kW	730 kW
Arm Cavity Finesse	450	450
Signal Recycling	$T = 20\,\%$, tuned	$T = 20\,\%$, tuned
Squeezing Factor	n.a.	20 dB
Filtercavity (FC) length	n.a.	300 m
FC Detuning	n.a.	-16.8 Hz
FC Input Mirror Transmittance	n.a.	425 ppm
Squeezing Losses	n.a.	9 % + 30 ppm roundtrip in FC
Test Masses and Suspensions		
Mirror Material	Fused Silica	Fused Silica
Main Test Mass Diameter	35 cm	55 cm
Main Test Mass Weight	42 kg	160 kg
Masses in Main Quad (from top)	22 kg/22 kg/40 kg/40 kg	44 kg/66 kg/120 kg/160 kg
Masses in Reaction Chain (from top)	22 kg/22 kg/40 kg/40 kg	22 kg/22 kg/40 kg/40 kg
Total Mass of a Main Suspension	250 kg	520 kg
Length of Final Suspension Stage	0.6 m	1.2 m
Fused Silica Fibre Diameter	400 μm	566 μm
Fibre Diameter at Bending Point	800 μm	1624 μm
Coating Noise Reduction		
Improvement Factors	n.a.	factor 1.6 from increased beam size + factor 2 from either better coatings, **OR** Khalili cavities, **OR** waveguides
Operation Temperature	290 K	290 K
IM/EM ROC	1934/2245 m	1849/2173 m
IM/EM spotsize	5.31/6.21 cm	8.46/9.95 cm
Khalili cavity length	n.a.	50 m
Gravity Gradient Noise		
Assumed Seismic Level	???	LLO ETMX, 90th percentile
Assumed subtraction factor	n.a.	5

The resulting sensitivity improvement in respect to the Advanced LIGO baseline is shown in the lower subplot of Figure 2. For all frequencies above 50 Hz the Strawman Red sensitivity can provide an improvement of a factor 3. In the range from 8 to 30 Hz the improvement is about a factor 4. The sensitivity curve presented here corresponds to an binary neutron star inspiral range of 614 Mpc.

2.3 Potential modifications to the Red Team Design

As was stated earlier the Team Red Design resulted from a certain set of input parameters (see section 2.1). In case other input parameters are to be used there are a few interesting modifications of the Team Red Design available that seem worthwhile to be explored.

In the following we give a brief description of a few potential design options:

- **Increased Circulating Power:** In case it is found that future thermal compensation systems can provide sufficient performance the interferometers could be operated with powers beyond 1 MW. If we for example assume that 3 MW of circulating power could be achieved (this is the design value for the Einstein Telescope room temperature interferometer) then this would allow us to improve the Team Red sensitivity by a further factor of $\sqrt{3/0.8} = 1.95$ for all frequencies above a few 100 Hz. Obviously this would come at the cost of increased radiation pressure noise at low frequencies.

- **Only Applying Mature Technologies:** If we are prepared to do without the magic factor of two in coating noise reduction (that we have considered to originate from either improved coatings or Khalili cavities or waveguide mirrors), then we would have a design include techniques and know-how that we already have! In principle we could start building such an interferometer right away. Such a detector would still provide a substantial sensitivity improvement (the only difference to what is shown in Figure 2 would be that the red trace would lie a factor 2 higher).

- **Xylophone:** So far we have only considered concepts in which a single interferometer covers the full frequency range of interest. However, it seems likely that at some point we will come to the point where it will be easier (in terms of complexity) and cheaper (in terms of cost and time) to build two simpler interferometers (each optimised for the noise sources relevant in its frequency range) rather than one extremely complex instrument (optimised for 'everything').

  Therefore, the baseline design of the Einstein Telescope consists of a 2-tone xylophone interferometer [2]. A high-power room temperature interferometer covers the high frequency range, while a cryogenic low-power interferometer covers the low frequency range. Such a concept resolves on one hand the problem noise sources scaling in opposite direction (e.g. shot noise versus radiation pressure noise), but on the other hand also eliminates the challenge of high power laser beams on cryogenic test masses.

  Figure 3 shows the extension of the Team Red design to a xylophone with parameters similar to the ET-D design [3]. The low frequency detector uses silicon test masses at a temperature of 40 K and a low optical power of only 18 kW. The xylophone would allow us to obtain a significant sensitivity improvement in the region between 5 and

50 Hz. (Please note that the exact level of low-frequency improvement will depend strongly the achievable mitigation/subtraction of other noises such as gravity gradient noise.)

- **Speedmeter:** As we have described in Appendix A of LIGO-T1200005-v2 a speedmeter topology could prove to be a viable option in case quantum radiation pressure noise requires significant suppression. This could for instance be the case if light powers above 1 MW will be used (see item above). Another scenario which would favour a speedmeter configuration over a standard Michelson interferometer is the case when test masses of lower weight have to be used. This could happen because of the limited maximal test mass size commercially available or because the seismic isolation and suspension systems can only carry test masses up to a certain weight. It has been shown theoretically that a speedmeter is able to provide the same low frequency quantum noise level as a Michelson interferometer for identical light power, but much lighter test masses.

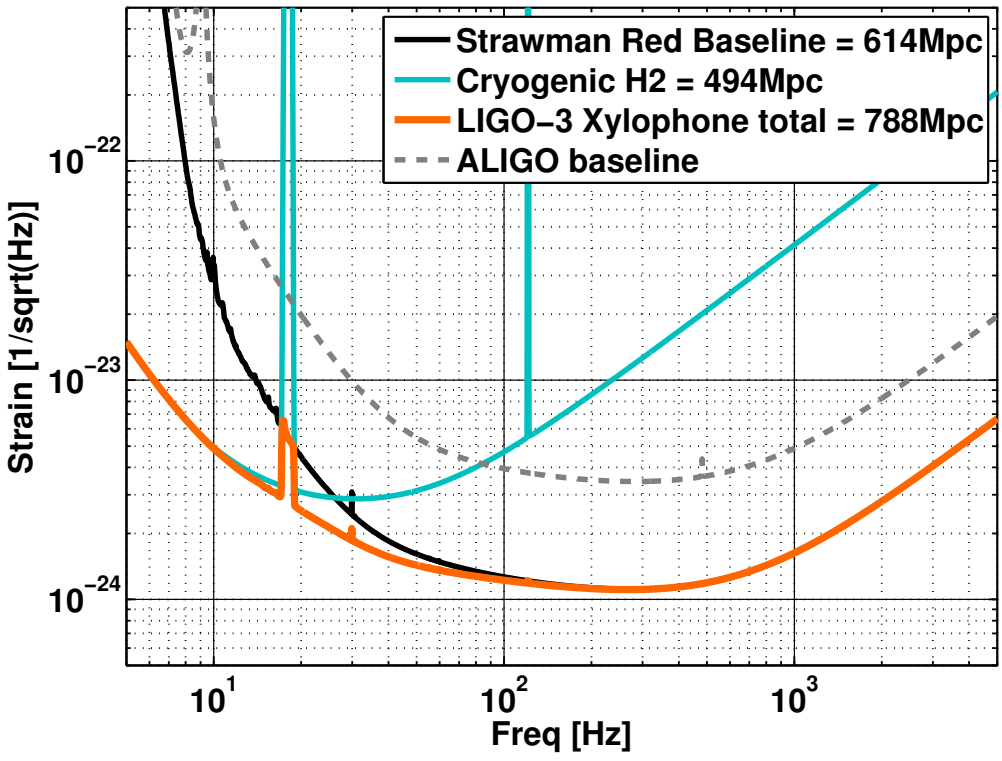

Figure 3: Sensitivity of a potential xylophone detector, consisting of a Team Red design interferometer (see Figure 2 and Table 1) covering the high frequency range and cryogenic, low-power interferometer covering the low frequency part. The cryogenic interferometer uses silicon test masses at a temperature of 40 K and a optical power inside the arm cavities of only 18 kW.

3 Blue Team Design

This design replaces much of the aLIGO interferometer with a new detector operating at 120 K.

- 150 kg Silicon mirrors at 120 K. (take image from COMSOL FEM)
- New quadruple suspensions to handle the increased mirror mass (add SolidWorks drawing from Calum).
- Silicon ribbons (and perhaps blade springs) in the final stage suspension at 120 K. (add dimensions from breaking stress calculation + add thermal conduction numbers)
- 1560 nm wavelength lasers operating at 300-700 W. Arm cavity powers of 2-5 MW. (info here about power recycling factor)
- Newtonian noise substraction via seismometer arrays and adaptive filters as described in P1200017 [4].
- Incremental improvements to the seismic platforms and structures: wires to stiffen the piers and chambers. Better sensors. More damping in the ISI.
- Epitaxial coatings (on the test masses only) for a mirror thermal noise improvement of 3-10x. Include information on AlGaAs and AlGaP and AlGaN hetero-structures.
- Squeezed light injection (10 dB) and a 100 m filter cavity for frequency dependent squeeze angle.

3.1 Choice of Silicon Mirrors

The Blue design is centered around the choice of silicon mirrors and has the aim of making a broadband noise improvement.

At cryogenic temperatures, the thermal conductivity of Si is hundreds of times larger than that of room temperature fused silica; this greatly suppresses the temperature gradients in the mirror and reduces the level of thermal compensation required.

At room temperature, the thermo-elastic fluctuations of the silicon substrate would prevent any sensitivity improvements. This, and the expected improvements in Brownian thermal noise, lead to cryogenic operation. The thermal expansion coefficient of silicon goes to zero at ∼120 K, ∼18 K, and 0 K [5] and so we should compare the interferometer sensitivity for both the 18 and 120 K temperatures.

Both the 18 and 120 K working points are possible, but there is less complication in operating at 120 K. At this temperature, ∼3-10 W of heat may be extracted radiatively (for an initial report on a cryogenic setup for this design see T1200093 [6]). At 18 K, all of the heat must be extracted through the fibers: this leads to a severe limit on the allowed cavity power and pushes towards using thicker fibers.

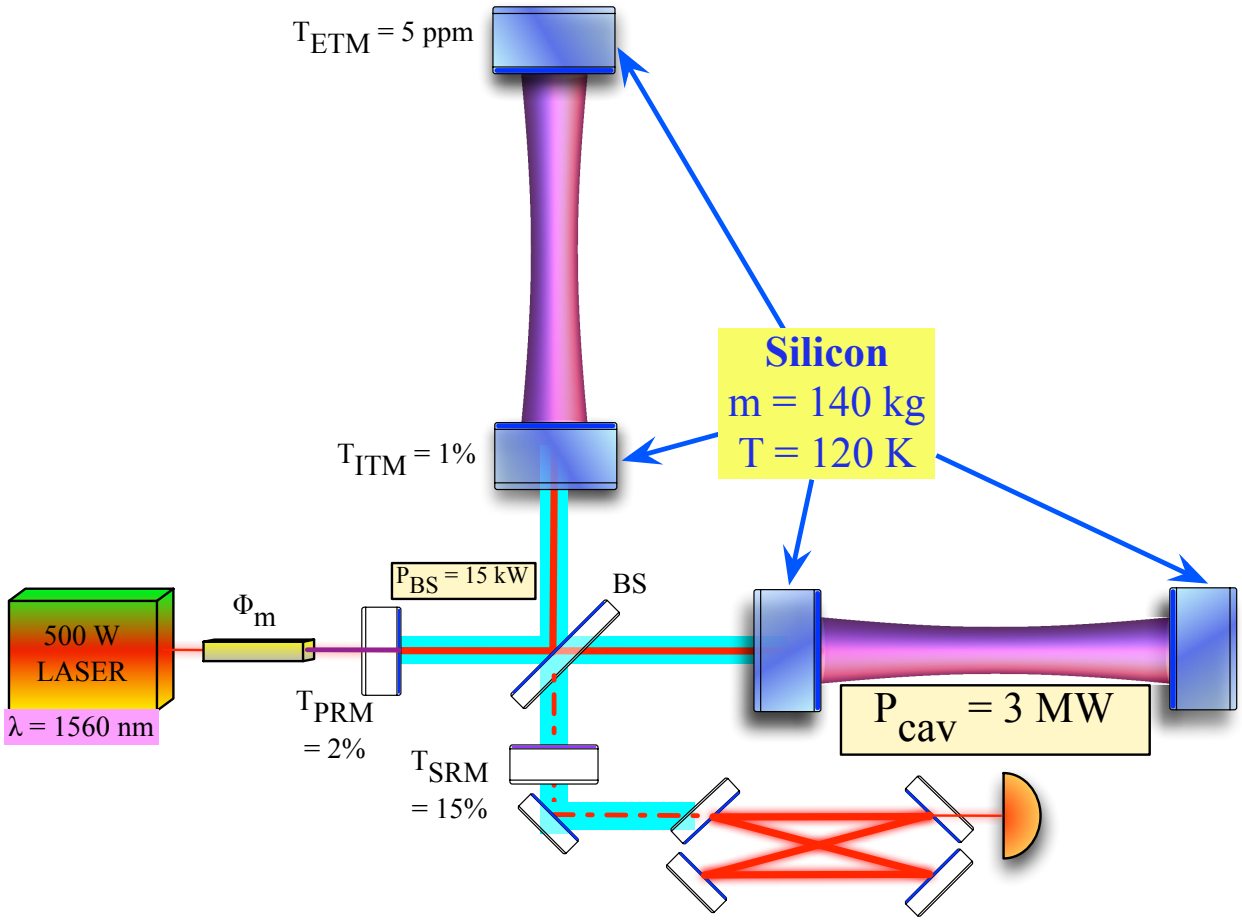

Figure 4: Schematic of the Cryogenic Silicon design

As silicon has a high absorption at 1064 nm, the laser wavelength is chosen to be 1560 nm (1560 instead of 1550, so that the Rubidium line at 780 nm may be used in conjunction with SHG for laser frequency stabilization). All of the silica optics will have to be replaced with optics coated for 1560 nm instead of 1064 nm.

3.2 High Power Possibilities

In the Blue design, the limit to the maximum stored power in the interferometer (ignoring high power control and alignment issues) may be determined by (a) the maximum power that can be extracted in cryogenic operation and (b) the maximum correction that can be applied by thermal compensation.

3.2.1 Cooling Strategy

We start with an assumption that the optic loses power largely through radiative coupling to the cryogenic environment (see Figure 7). If the optic is held at 125 K and the environment is 77 K, then, approximately 4 W of power is radiated (for total surface area of $1m^2$ and an emissivity of 0.33). If no other cooling mechanism is in place, the maximum absorbed

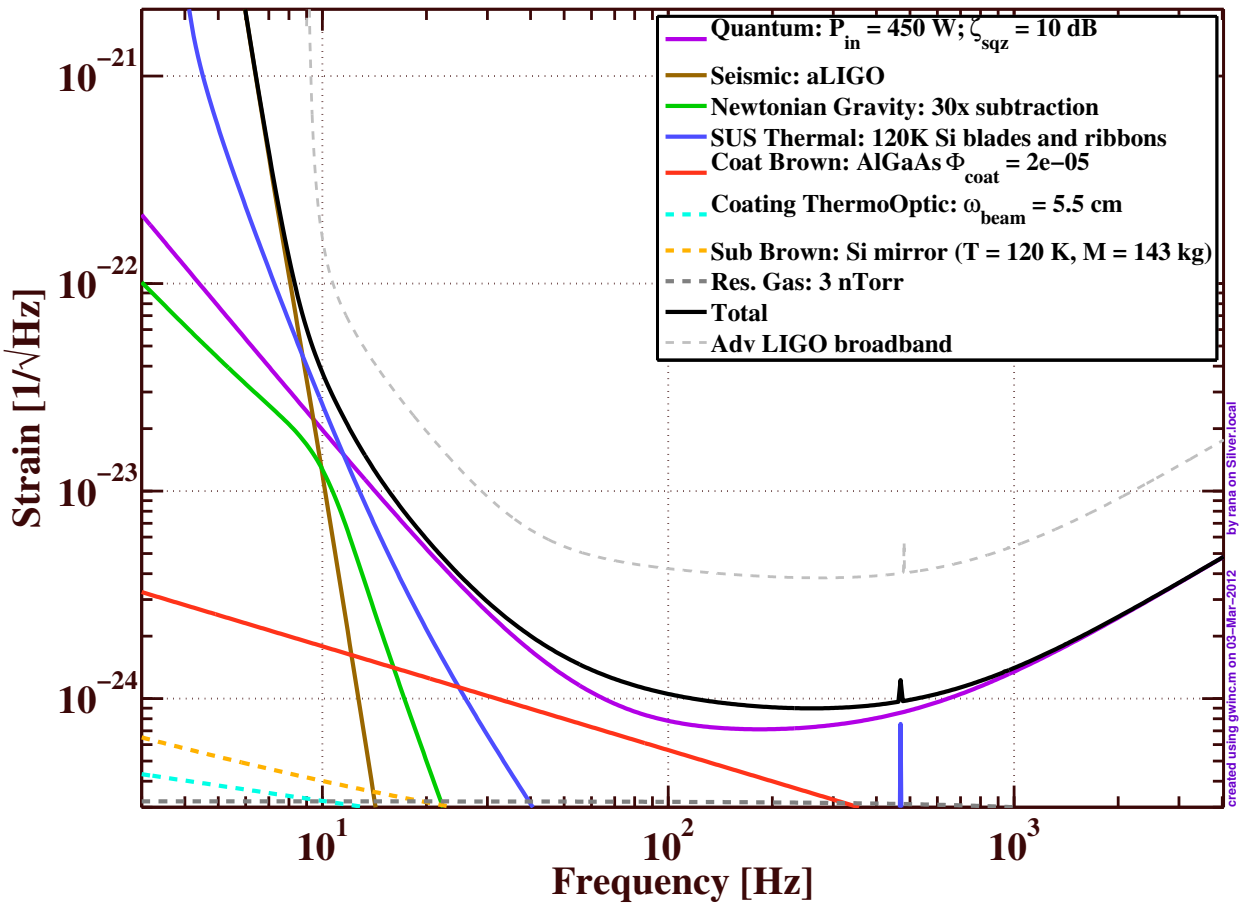

Figure 5: Noise Breakdown of the Blue Team design

power in the optic cannot exceed 4 W to keep the optic temperature at 125 K. The conductive cooling capacity of the silicon suspension ribbons should add somewhat to this cooling power.

If we assume that all of that 4 W heat load is due to absorbed laser power, then the maximum incident power on the optic cannot exceed 4 W*(1/substrate absorption + 1/coating absorption). For AlGaAs coatings, the best coating absorption measured is 7 ppm [7]. If we assume that this can be improved by a factor of $\sim$ 10 over the next decade, then the coating absorption would be $\sim$1 ppm (including contamination). If we assume substrate absorption is negligible then the maximum possible interferometer power would be $\sim$8 MW.

3.2.2 Thermal Compensation

The thermal lens in a silicon test mass absorbing 10 W interferometer power has a characteristic size of almost the same scale as the thermal lens in aLIGO. If we use a compensation plate (see Figure 7) to correct for the thermal lens/optical path distortion (OPD), then the following information is useful in determining the solution:

The positive thermal lens scale factor (from self induced OPD) is 20 nm/W for silicon and

500 nm/W for fused silica. The negative thermal lens scale factor (from corrective OPD) is 0.3 nm/W for silicon and 25 nm/W for fused silica. Therefore, to correct for 200 nm of OPD, a silicon compensation plate would require 750 W of compensating power, while a fused silica compensation plate would require only 9 W of compensating power.

We conclude:

- the maximum operating power is limited by the cryogenic operating condition (total absorbed power cannot exceed 4 W), not by the ability to correct for thermal lensing.
- The most efficient compensation system is one with a cryogenic silicon test mass and a cryogenic fused silica compensation plate, where the required compensating power is roughly 0.9 x the absorbed power.
- Lastly, a fused silica compensation plate with $1m^2$ surface area that also sees a 77 K environment absorbing 9 W will have an average temperature of 122 K and will thus not overly burden any cryogenic system.

3.2.3 Cryogenic Suspension

Choice of Mirror Mass Increasing the mirror mass, linearly reduces the radiation pressure noise. In addition, the suspension thermal noise is reduced due to the relative surface to volume ratio effects.

It is now possible to produce silicon boules with the approximate dimensions required to make a 150 kg test mass, The 150 kg number is a first guess at what may be possible to suspend without exceeding the mass limits of the existing seismic isolation platforms. The quadruple suspension will have to be redesigned to accomodate such a large mass.

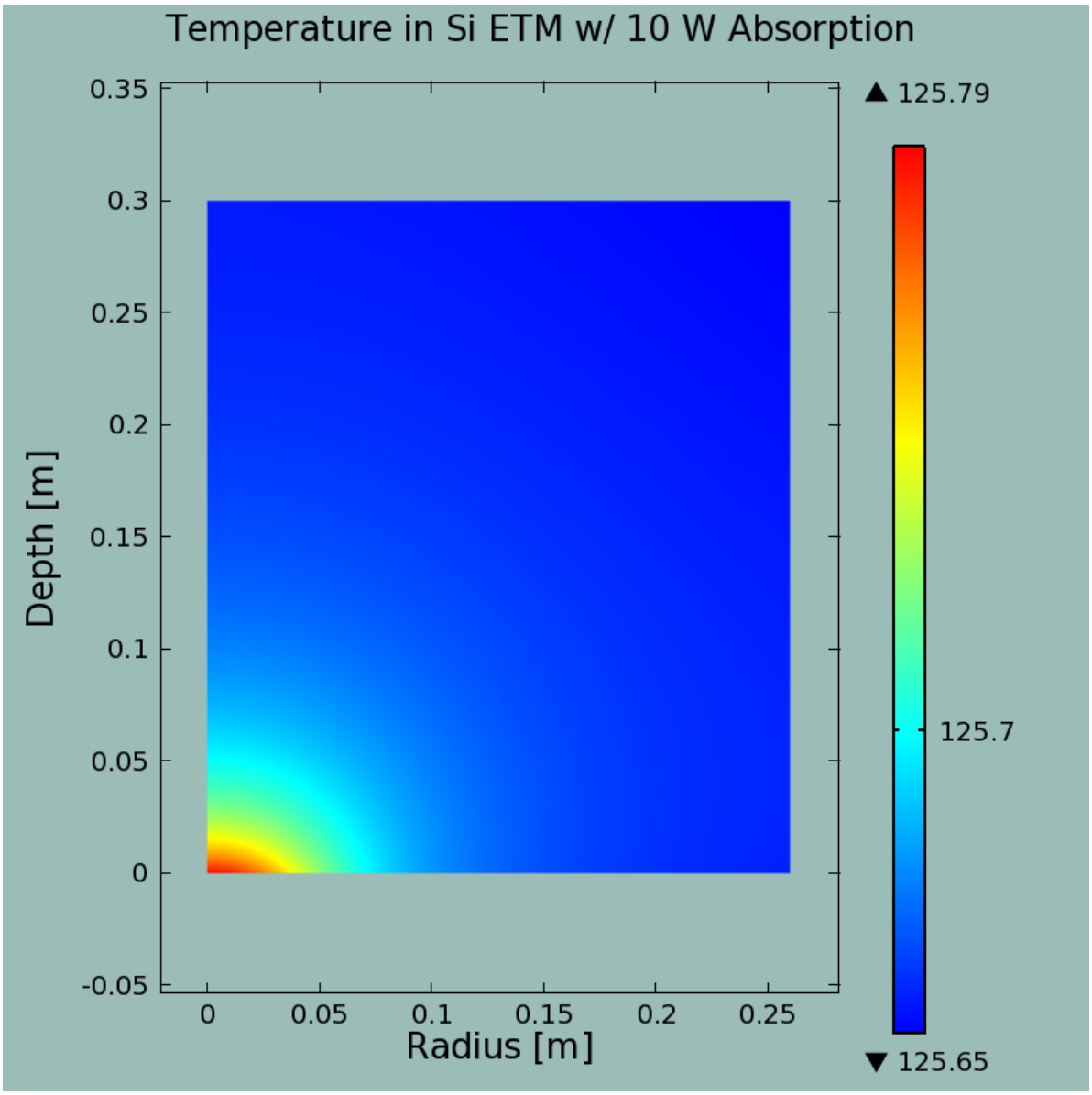

Figure 6: COMSOL FEM of 10 W heat load from a $\omega = 5$ cm Gaussian beam on a 120 K Si mirror

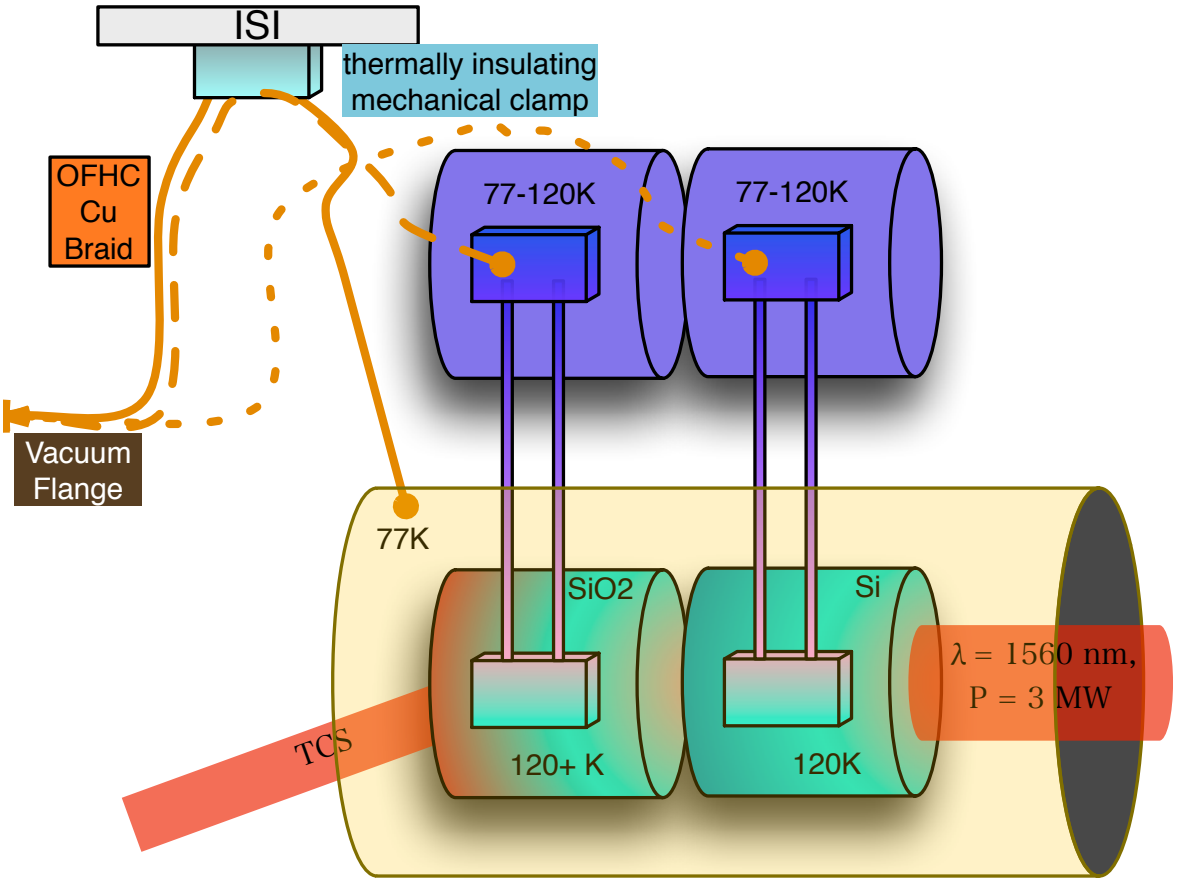

Figure 7: A cartoon illustrating radiative and conductive cryogenic cooling of a Silicon test mass and SiO2 compensation plate.

4 Green Team Design

The green team investigated two distinct design ideas:

- Combining the ideas of Fabry-Perot cavities and Herriott delay lines, forming resonant delay lines.
- The use of a suspension point interferometer on the penultimate mass (or separately suspended from the penultimate mass) as high frequency interferometer of a xylophone. The low frequency interferometer remains on the (ultimate) test mass.

Other design elements are copied or compatible with ideas from the other groups. These are

- baseline design with 1064 nm laser and silica optics at room temerature, but compatible with cryogenic operation at 1560 nm wavelength,
- 160 kg test mass
- improved suspension for a reduction in suspension thermal noise
- Newtonian noise substraction via seismometer arrays
- Squeezed light injection (10 dB) and a 100 m filter cavity for frequency dependent squeezing.

4.1 Resonant Delay Lines

The primary reason for exploring this configuration is the desire to increase the sampled surface area of the optic to reduce the coating Brownian noise. Following the idea of a Herriott delay line, arranging the spots in a cricle should simplify the optics design. In contrast to the Herriott delay line, the beam path is closed into a Fabry-Perot cavity after N trips. Such multiply folded arm cavities can be built in either travelling wave or standing wave configuration.

4.1.1 Traveling Wave vs. Standing Wave Resonant Delay Lines

Travelling wave cavities have the advantage that all the reflection spots are only sampled once, reducing the coating Brownian noise correlation between individual reflections. They however make it more difficult to separate the input and output beam in the central interferometer and and to provide a power and signal recycling path.

The double-sampling that occurs on all folding spots in a standing wave resonant delay line introduces maximum thermal noise correlation for pairs of reflections sharing the same location. This apparent disadvantage is hovever compensated by the increased number of arm round trips for a given mirror surface area. Figure 11 shows that in terms of thermal noise there is actually very little difference between the two.

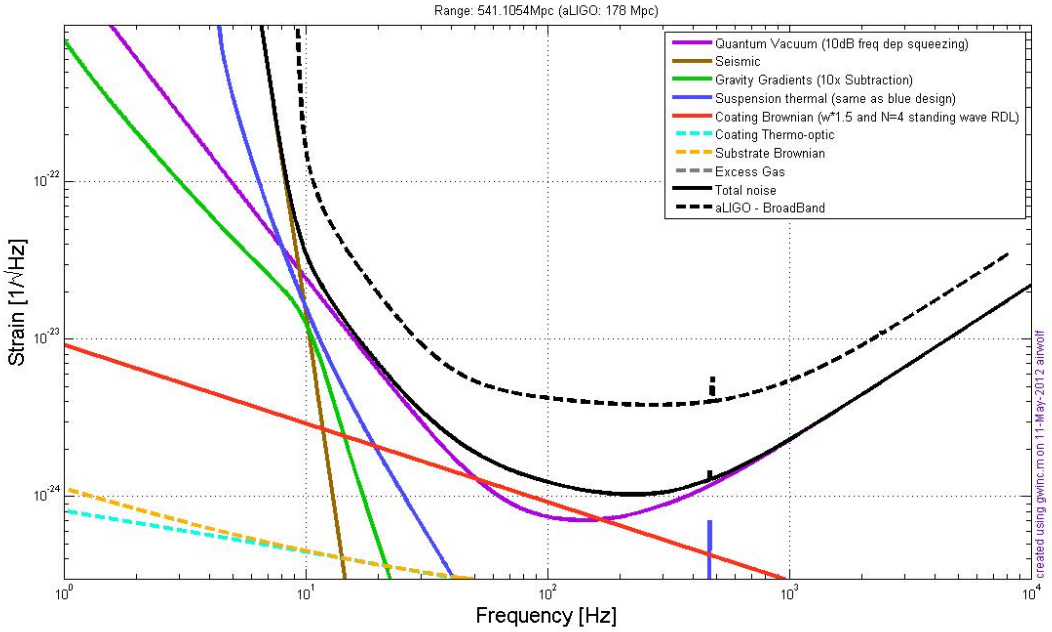

Figure 8: Example Green Design sensitivity. Standing wave resonant delay line with 4 spots per mirror, beam spot increase of w*1.5 over aLIGO, mass=160 kg, 10dB squeezing. For other parameters see table 3

4.1.2 Quantum Noise

For fixed arm power the shot noise calibrated in strain/rtHz below the cavity pole will improve linearly with the number round trips. Radiation pressure noise on the other hand suffers, as the optic is coherently driven by all reflections, and all refections sample the the mass motion. Thus a large mass is desired for both attaining a large front surface and reducing radiation pressure noise.

Also, assuming the optical loss per reflection is constant, the total arm loss will increase, requiring a higher input laser power to maintain the same arm power. However the increase radiation pressure noise and decreased shot noise actually lead to a lower optimal arm power.

4.1.3 Sensitivity at the Free Spectral Range (FSR)

The multiple folding brings the cavity free spectral range down to $FSR = \frac{c}{2*N*L_0}$, with N the number of reflections. Unlike an unfolded cavity, the sensitivity of a folded cavity to both mirror displacement and gravitational waves goes to zero at the FSR, see e.g. figure 12. The requirement to keep this sensitivity loss out of the sensitive band limits the number of reflections to about 10.

4.1.4 Residual Brownian Noise Correlation

The Brownian noise correlation of a delay line was analysed in [8], and is directly transferable to resonant delay lines in a Herriott configuration. The residual correlation even for non-

overlaping spots leads to a correction of order 10%, compared to a naive calculation. See figure 11 for details.

4.1.5 Mode size and alignment control

Several reasons force us to modify the simple Herriot delay line configurations with two spherical mirror slightly:

- Mode selection capability, i.e. higher order spatial modes should not be resonant.
- The desire to have a standing wave cavity for simplicity in the central interferometer.
- Mirror tolerances, i.e. the ability to compensate for mirrors with realistic figure errors.

Our current thinking is to modify two areas on the mirrors to from input and output coupler. At least one of them has to be on a separate mirror to allow forming a resonant cavity in the presence of realistic mirror figure errors. The effective radius of curvature of those mirrors can be used to avoid higher order spatial mode resonances. More research on this is needed.

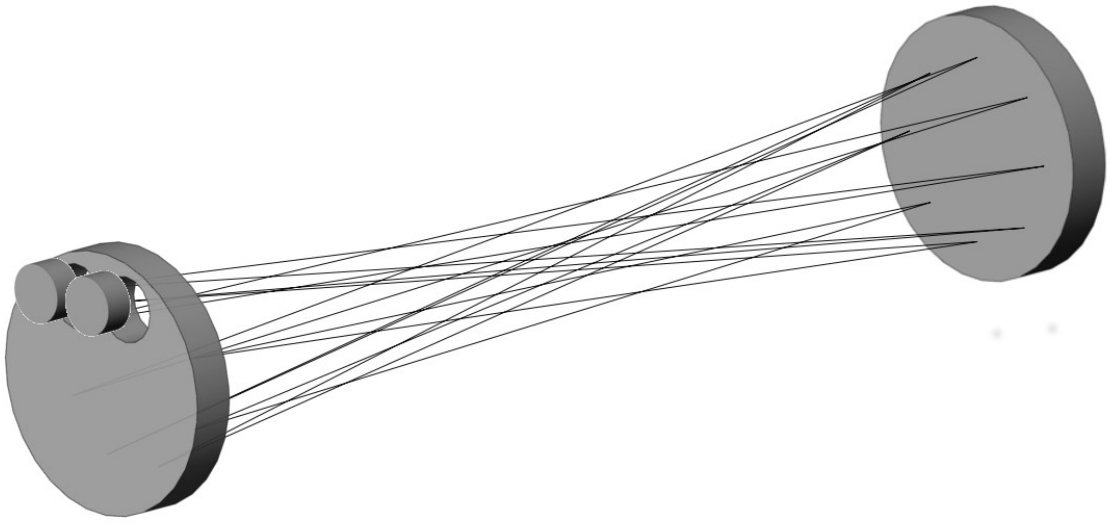

Figure 9: Configuration sketch for an 8 bonce traveling wave cavity. This configuration would reduce the thermal noise by a factor of 3 compared to a single bounce cavity.

4.1.6 Path-to-Path scattering

Path-to-path was one of the issues plaguing traditional delay lines. Using a resonant delay line configuration thus requires that, in addition to the cavity-round-trip distance, the mirror separation has to be controlled. If input and output coupler are part of the main mirrors, this happens automatically. Otherwise an adittional cavity in the center of the arm can be used for both locking and stabilization.

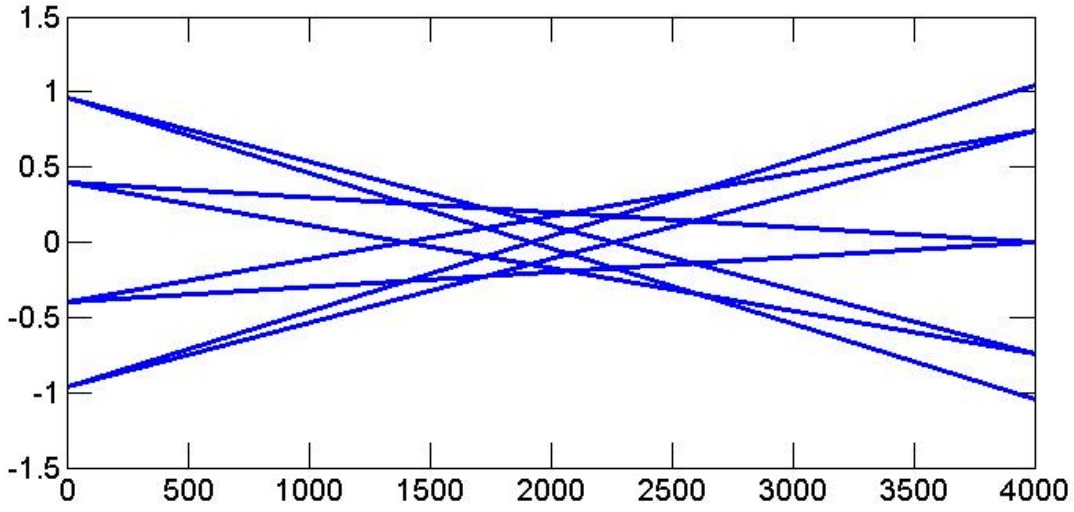

Figure 10: Beam path of a negative branch resonant delay line.

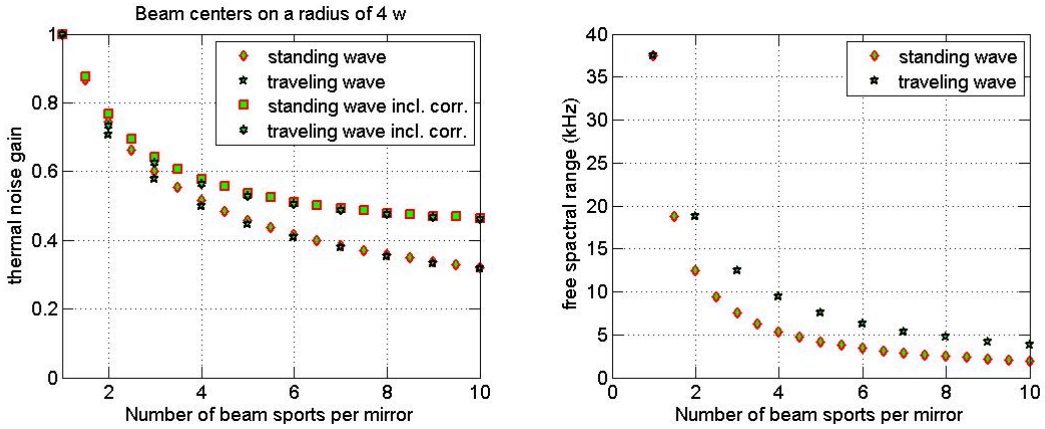

Figure 11: Thermal noise improvement factor and FSR as a function of number of bounces. The Brownian thermal noise corretion was estimated assuming all beam centers sit on a circle with radius 4 w and using the result from [8]. See the text for details.

4.2 Suspension-point interferometer (SPI)/Xylophone

4.2.1 Overview

The SPI proposed by the Green Team is actually a hybrid of two separate design methodologies. The traditional SPI (see, for example, [**?**]) uses an additional interferometer as a

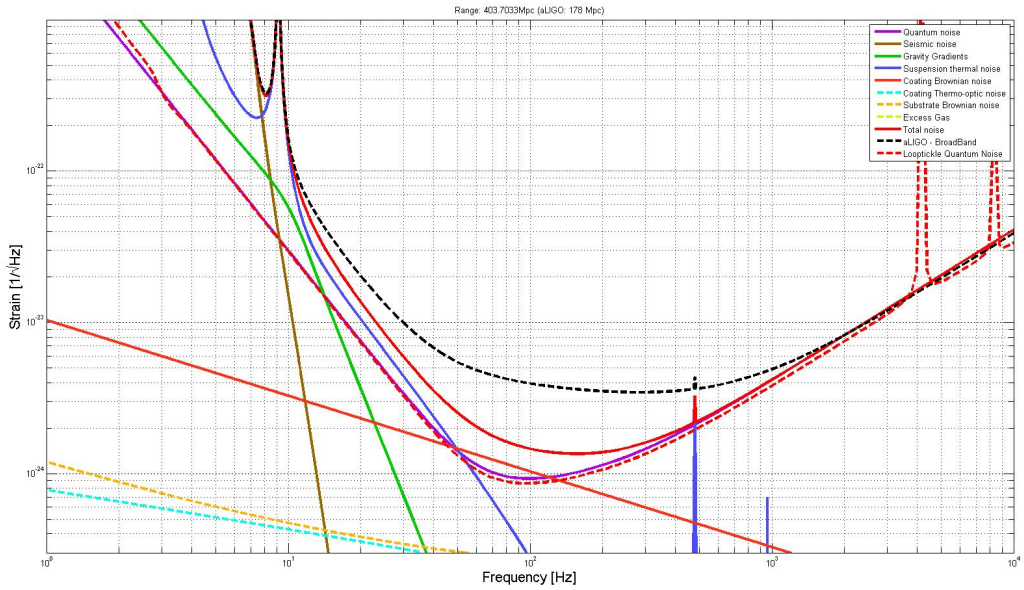

Figure 12: Example sensitivity for a traveling wave resonant delay line with 9 spots per mirror. Input Power=375 W, mirror mass=300 kg. The remaining parameters are idenical to aLIGO, including the individual beam spot size, the per bounce scattering loss and no use of squeezing. The suspension thermal noise is copied from aLIGO, i.e. it needs to be updated with an appropriate suspension model. Also plotted is the quantum noise calculated by looptickle/optickle, which includes the sensitivity loss ath the FSR.

sensitive displacement sensor on the penultimate (PUM) stage of the suspension. The error signal from this IFO is fed back to the PUM, in effect isolating the ultimate mass (UM) from any displacement noise that reaches it by way of the suspension chain. In practice, seismic noise is the most significant contributor of this type.

A different—but not completely independent—idea is to use this auxiliary IFO to sense gravitational waves, as well. By changing the parameters of the individual IFOs (e.g., mass, dimensions, laser power, etc.), the two detectors can be made to have optimal sensitivity in different bands. This type of multi-band IFO has been termed a "xylophone detector".

The "Green Hornet (GH)" SPI (Fig. 14) is a combination of these ideas. The PUM is made to have a lower mass than the UM, and the laser power of the upper IFO is higher than that of the lower stage. The result is that the upper IFO has better quantum-limited performance at high frequencies, where its lower shot noise dominates, while the lower stage prevails at low frequencies, where it is dominated by its lower radiation pressure noise. Finally, since the upper IFO is not used for GW detection at low frequencies, it can be used in this band as a sensitive displacement noise suppressor. The displacement noise fed through to the UM is then just the fully suppressed, closed-loop residual noise of the upper IFO, filtered further by the passive final pendulum stage.

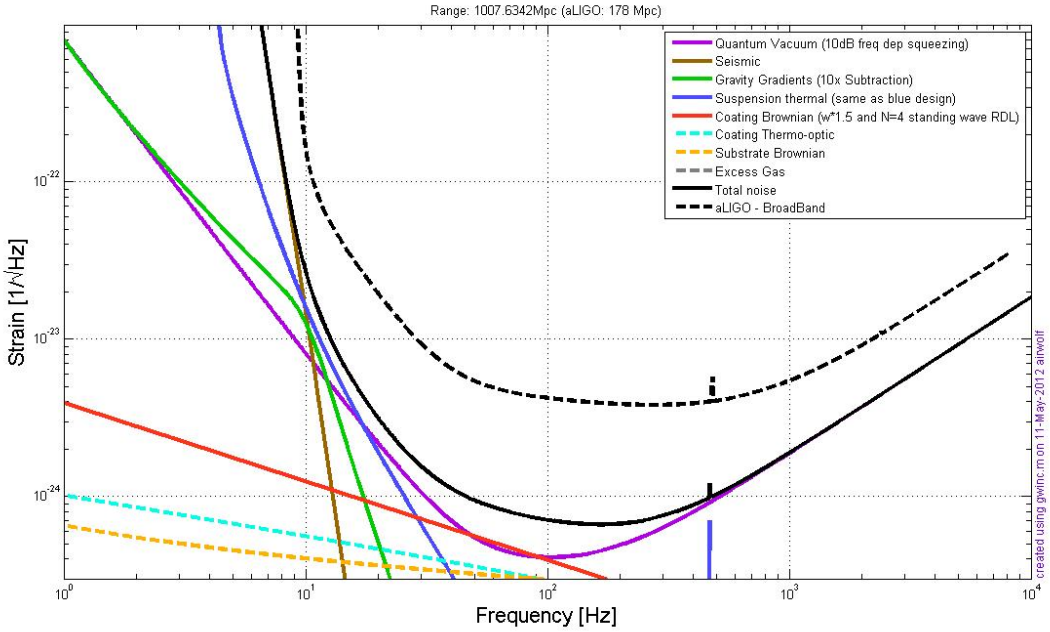

Figure 13: Example sensitivity for an extreme upgrade using a 9-spot traveling wave resonant delay line, 100 kg optics, 500 W of laser power.

4.2.2 Green Hornet modeling

To model the SPI, the gwincDev code was modified to reflect the appropriate mechanical system. Essentially, it was modeled as two independent interferometers, with various assumptions given the expected effect of the coupled system.

- **Upper IFO:** When calculating the noise of the upper IFO, the mass of the UM is artificially increased by 10^6 to simulate the effect of servo control of the lower IFO. Aside from this, the noise of the upper IFO is simply calculated as if there were an IFO on the PUM of an aLIGO-style suspension.
- **Lower IFO:** Simulation of the lower IFO requires no significant modification of the mechanical model. Its noise is calculated as usual for an IFO on a quadruple suspension, however the horizontal seismic noise is removed from the model, reflecting the suppression from the locked upper stage.

A collection of the parameters used in modeling the GH SPI can be found in Table 2. These are the result of an optimization for a crossover frequency of 140 Hz between the upper/lower IFOs. Note that frequency-dependent squeezing is only applied to the lower IFO; frequency-independent squeezing is used for the upper IFO.

The noise budget for this SPI is shown in Fig. 15.

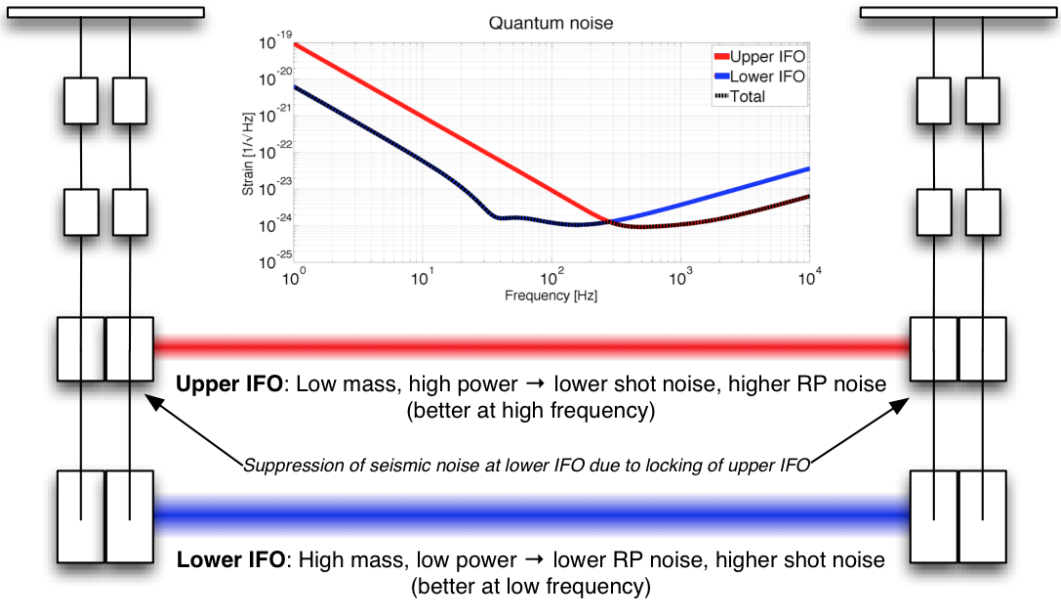

Figure 14: A cartoon of the SPI configuration. The upper interferometer comprises lighter mirrors and a higher-power beam, while the lower interferometer has heavier mirrors and a lower-power beam. The inset shows the quantum noise for each interferometer.

4.2.3 Independent control solution: dual ultimate mass "Wind Chime"

One concern with the traditional SPI is that small deviations from perfection in the welding of the suspension will lead to prohibitive misalignments between the two stages, as illustrated in Fig. 16. Each IFO will require $\sim \mu$rad pointing accuracy, and this would impose impractical welding tolerances.

In principle, one could use the actuators on the lower stage to apply DC pointing corrections. Since the lower IFO must be quiet at low frequencies, the plan is to use quieter (but weaker) electrostatic actuators in place of stronger magnetic actuators of the upper stages. These weaker actuators are not believed to be strong enough to counteract predicted hanging misalignments, and so another solution must be found.

In lieu of this design, another option is to simply have two ultimate masses suspended from a common PUM. In this case, there would be no IFO on the PUM stage. Each IFO could be tuned as usual, and the only further complication is the transfer function between the two IFO masses. An illustration of this setup can be found in Fig. 17.

Modeling of the dual-UM

Some very preliminary analysis of the dual-UM concept has been done. Aside from some extra constraints on the upper mass (UM1) dimensions due to the finite size of the beam tube, we are still free to choose the individual IFO parameters as we wish to tailor the overall quantum noise. Therefore, the benefit of the xylophone configuration is largely recovered.

The same is not trivially true for the displacement noise suppression enjoyed by the tradi-

	Upper IFO	Lower IFO
Mirror mass [kg]	13.82	156.8
Input power [W]	250	50
PR gain	119.3	167.4
BS power [kW]	29.8	8.4
Arm finesse ($\mathcal{F}$)	158	111
Circulating power [kW]	1503	295
Mirror radius [cm]	10	27.5
Beam size (ITM/ETM) [cm]	(4.0/4.0)	(11.0/11.0)
ITM transmission	0.0396	0.0566
PRM transmission	0.0084	0.0060
SRM transmission	0.2587	1.0000
SRM detuning [rad]	0.0030	0.0000
Squeeze amplitude [dB]	20	20
Squeeze angle [rad]	0.0268	0.2713
Filter cavity length [m]	N/A	100
Filter cavity T_i	N/A	1.9×10^{-4}
Filter cavity T_e	N/A	5.0×10^{-9}
Filter cavity rotation [rad]	N/A	-0.2929

Table 2: Parameters used for the Green Hornet SPI simulation.

tional SPI. The usual scheme works because the PUM, which acts as the suspension platform for the UM, is rigidly locked in place. In the dual-UM case, the locked upper IFO is no longer the support for the lower IFO, but rather they share a common PUM. As we will see, the suppression can be recovered substantially by distributing feedback control of the upper IFO both locally (to UM1 itself) and to the PUM. The predicted performance of a dual-UM SPI/xylophone with no suppressive feedback is shown in Fig. 18. Note that the performance is nearly identical to that of the standard GH design above ∼10 Hz. Below this, unsuppressed seismic noise makes it significantly worse.

Below the resonant frequency of its supporting pendulum, UM1 is well coupled to the PUM. In fact, up to an even higher frequency, the displacement noise of UM1 is completely dominated by noise fed through to it from the PUM. This means that, with competent filter shaping, the upper IFO can be locked at these low frequencies via feedback to the PUM, thereby also suppressing the noise that would be fed through to UM2 (the lower IFO). Figure 19 shows the expected low-frequency noise budget for both the PUM and UM1. Of note is that the UM1 noise is dominated by seismic feedthrough up to ∼6 Hz. Aggressive feedback can therefore be applied from the upper IFO to the PUM position below this frequency, resulting in the suppression of UM2's motion. As shown in Fig. 20, the full advantage of the SPI/xylophone can be attained with this feedback in place.

Caveats and issues to be studied further

The following is a list of issues that must be addressed for the dual-UM analysis to really be

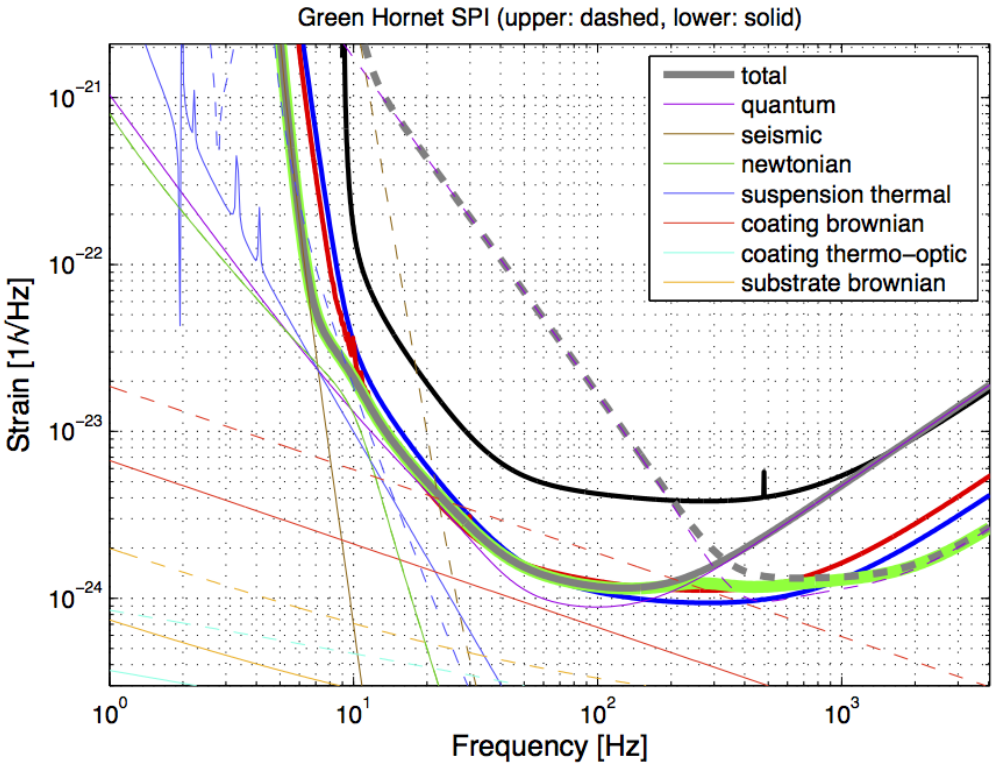

Figure 15: Noise budget for the Green Hornet SPI, given the parameters in Table 2. Traces for the upper IFO are dashed and those for the lower IFO are solid, and the total combined GH noise is in thick solid green. The thick blue and red curves are the Blue and Red team noise curves, respectively, and the thick black curve is the aLIGO broadband noise curve.

trusted:

- **Suspension mechanics**: Whereas the GH modeling could be done relatively simply by modifying the quad suspension model, an extra degree of freedom must be added to the model to account for the fifth mass. This is straightforward, but not trivial or quick. So, the preliminary modeling was done independently for each UM, ignoring the effect of the other mass in each case.

- **Dimensional constraints**: The finite size of the beam tube restricts the dimensions of the UMs. Due to the xylophone concept, UM2 ought to be as large as possible. These simulations were done for an UM2 of $R_{UM2} = 25$ cm, on a suspension of the aLIGO length ($L_{UM2} = 0.6$ m). The PUM was chosen to have the same dimensions as that of aLIGO ($R_{PUM} = 17$ cm). Leaving room for 1 cm of spacing between UM1 and UM2/PUM, this leaves room for an UM1 of $R_{UM1} = 8$ cm, which is quite small.

  The upper IFO is not anywhere limited by coating thermal noise, and therefore there is no strong noise dependence on the size of the beam. Geometrical stability and clipping losses must however be taken into account, and so a careful optimization of the size ratio between UM1/UM2 should be conducted.

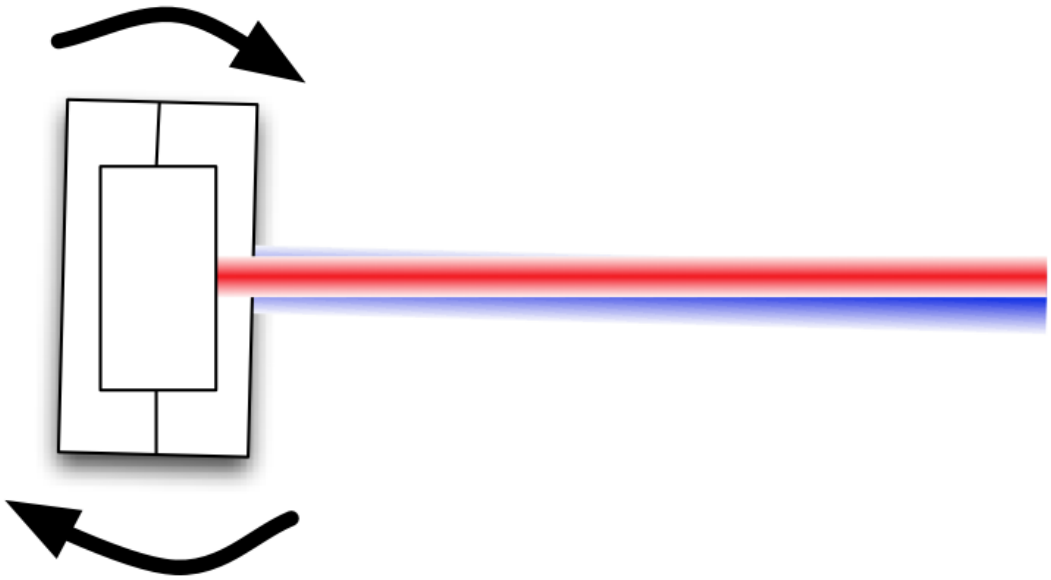

Figure 16: Illustration of the misalignment between stages that can result from imperfect welding.

4.3 Some additional technology investigation

LG33

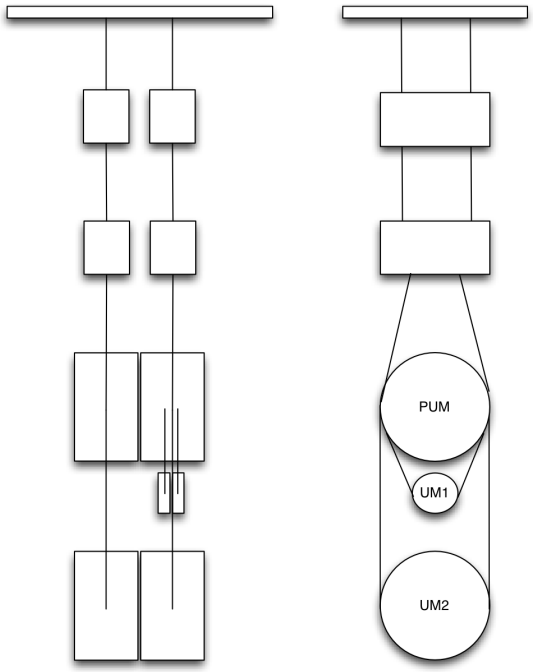

Figure 17: Illustration of the dual-UM concept. The first three stages from the top are standard and have no interferometric readout. From the third stage (PUM), two separate ultimate stages are hung, each with its own IFO.

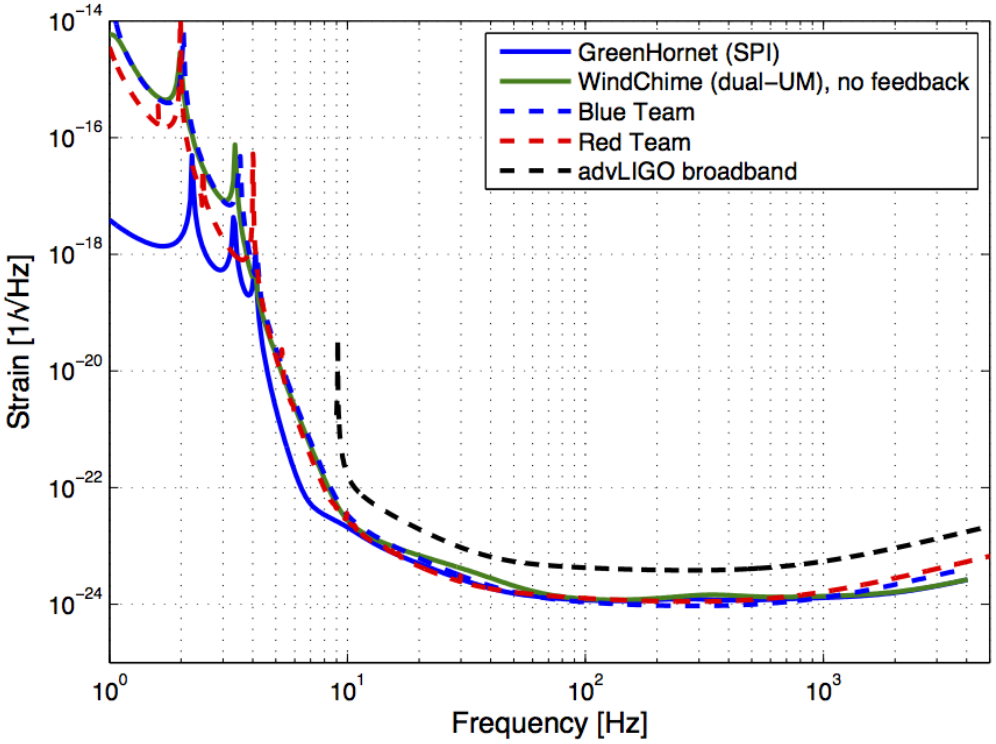

Figure 18: Predicted performance of the dual-UM SPI/xylophone with no suppressive feedback, in comparison with the traditional SPI configuration (GH) as well as the Blue Team, Red Team, and aLIGO designs.

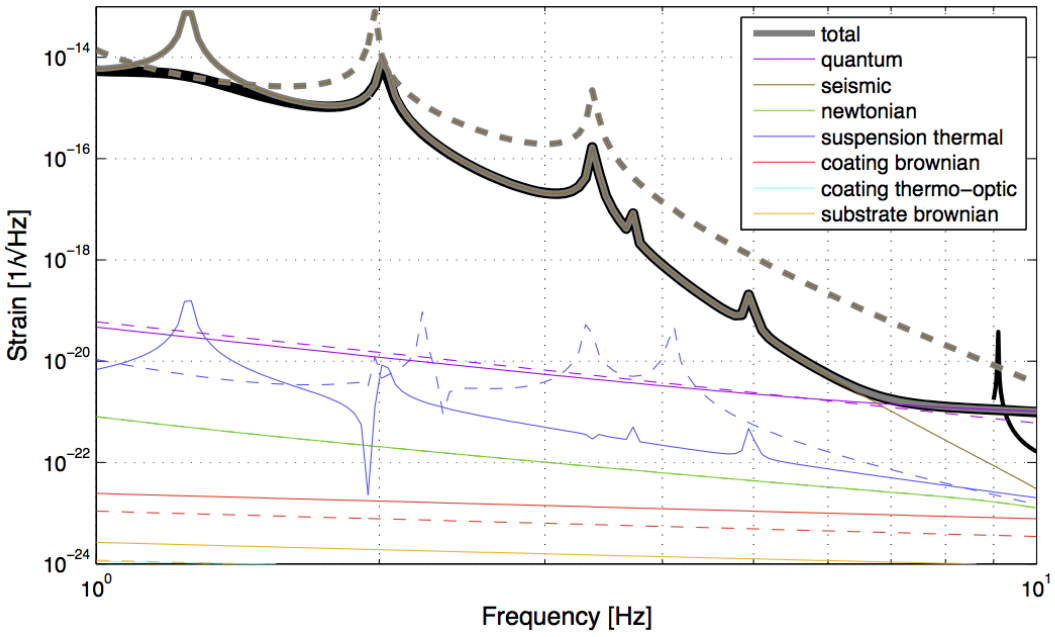

Figure 19: Expected low-frequency displacement noise of the PUM (dashed) and UM1 (solid) stages. Below ∼6 Hz, the noise in UM1 is dominated by the noise in PUM, filtered passively by the pendulum by which they are connected.

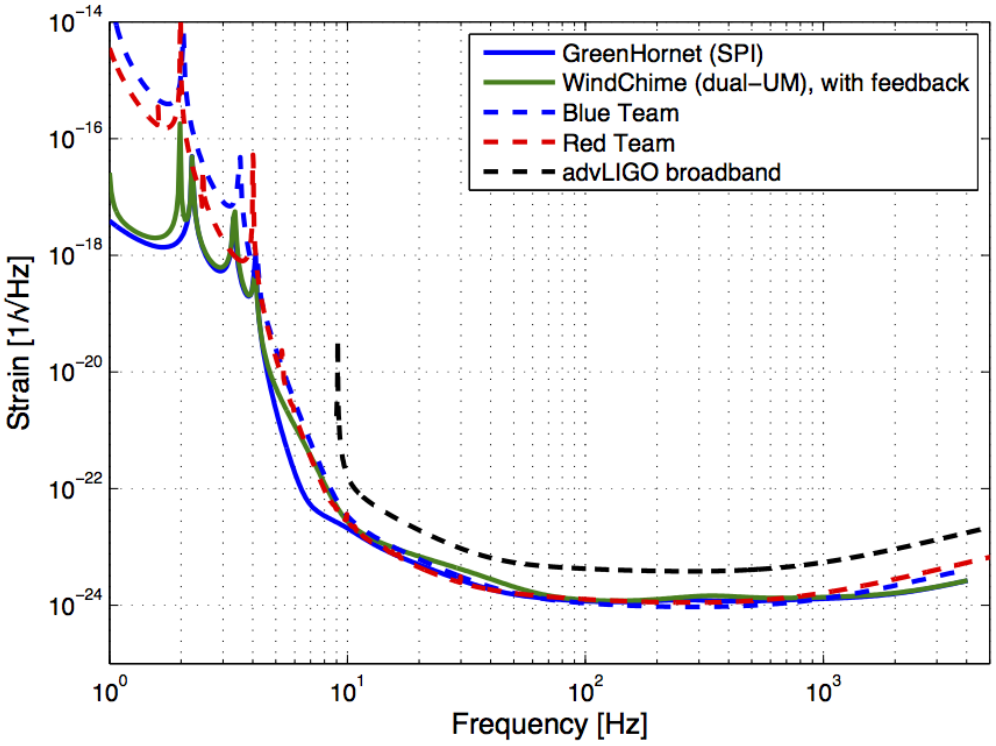

Figure 20: Predicted performance of the dual-UM SPI/xylophone with suppressive feedback from UM1 to the PUM, in comparison with the traditional SPI configuration (GH) as well as the Blue Team, Red Team, and aLIGO designs. The performance of the traditional SPI is almost completely recovered.

5 Comparison of Detectors

IFO Cases	Blue	Red	Green	aLIGO	ET
Mirror Mass [kg]	143	160	160	40	
Mirror Material	Silicon	Silica	Silica	Silica	
Mirror Temp [K]	120	295	295	295	
Sus Temp [K]	120	295	295	295	
Sus Fiber	0.6m Si - Ribbon	1.2m Silica fiber	TBD	0.6m Silica fiber	
Input Power [W]	450	125	125	125	
Arm Power [kW]	2800	800	210	800	
Wavelength [nm]	1560	1064	1064	1064	
NN Sub	30	5	10	1	
Coating Type	AlAs:GaAs	SiO:TaO	SiO:TaO	SiO:TaO	
Beam Size [cm]	5.3 / 6.2	8.5 / 10	8.3 / 9.3	5.3 / 6.2	
SQZ Factor [dB]	10	20	20	0	
F. C. Length [m]	100	300	100	N. A.	

Table 3: Baseline parameters for aLIGO and the Strawman IFO configurations

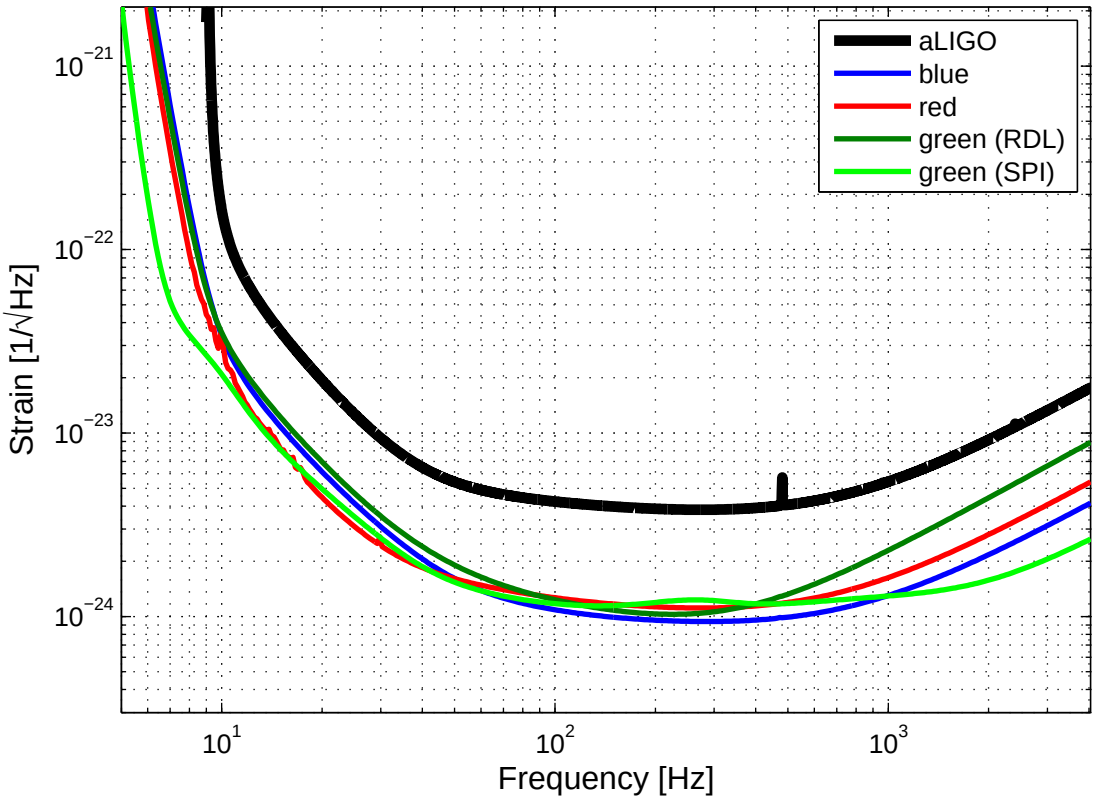

Figure 21: Comparison.

6 Research Plan to Support the Strawman Designs

While the Strawman Designs will require some common research for the development of their subsystems for the most part they will require different levels of research effort for the development of their various subsystems. We will now discuss the Research and Development effort that will have to be undertaken before the building of each of the different Strawman Design subsystems can begin.

6.1 Suspensions

The Red, Green and Blue designs will all require new quadruple suspension systems (SUS) designed to support the much heavier test masses. (The Internal Seismic Isolation (ISI) team believes it can by eliminating some ISI ballast mass allowing more suspension system mass.) The two upper stages will continue to be made of steel with steel wire suspensions in all three designs and the attachments will likely continue to be done with metal fasteners as well. Modeling and engineering work will be required to produce optimum mass distribution (with a fixed total mass determined by the ISI subsystem) in the suspension chain for all three designs. It will probably be necessary to investigate the losses in attachments (either bonding or welding) in all of the lower two stages (penultimate and testmass) suspension designs. In a new quadruple suspension design with improved vertical isolation and lower thermal noise the existing triple suspensions in the recycling cavities may then need to be upgraded. We will now describe the Research and Development work required that is not common in the Red, Green and Blue designs. The heaver suspension cartridges could requireadditional engineering work on improved tooling, fixtuing and procedures.

6.1.1 Suspensions for the Red Design

As written above, the Red Design will require research and development into a design which can support a 160 kg core silica optic and an approximatie doubling in the diameter of the final stage silica suspension fibers. It may be necessary to redesign the neck of the silica suspension fiber to produce the desired dissipation dilution factor. This will require additional FEA of the fiber neck to achieve a more precise understanding of thermoelastic cancellation. To achieve a longer suspension for a heavier mass the stress in the fiber may have to be increased which will require testing to failure to determine the breaking stress and laboratory prototyping. Further study of ways to improve the welding process of fiber to attachment ear will need to continue with a focus on mechanical loss and creek noise. Additional work is needed to optimize the mass values of the quadruple main suspension chain and reaction chain. The effect on local damping, resonant modes and control authority needs to be fully investigated through simulation.

The techniques necessary to pull and weld 5 mm diameter fused silica fibers with sufficiently short neck and stock needs to be further developed. Initial tests appear promising but suitable tooling and an extension to the pulling machine need to be proven. Furthermore, the possibility of using a factor of 2 higher stress in the fibers must be fully assessed and the parameter space explored.

The use of improved OSEM sensors (e.g., the EUCLID interferometric device) needs to be

fully assessed for reducing sensing noise in the quadruple pendulum. Finally a re-design needs to be done on the quadruple suspension hardware such as interface plates, metal masses, wirejigs, cantilever springs and catcher structures.

6.1.2 Suspensions for the Blue Design

For the Blue Design much of the work described above for the Red design will also need to be done. In addition, it will be necessary to design and build a more or less new suspension from different materials in the final stages. These new materials include silicon fibers or ribbons in the final suspension stage which can operate at 120 K and silicon core optics. Semiconductor grade Silicon boules of sufficient size are being grown today but fabrication or growth methods for the silicon fibers will have to be developed with a particular to the methods that maintain the high Q of the materials. The use of laser growth techniques would need some development because of the issues related to the change of the optical absorption at 10 microns of silicon upon melting. The more likely route to develop these fibers will involve etching bulk silicon rods, a standard approach, but not one currently used to produce fibers of this length or thickness. The oxide layer typically on silicon makes it a good candidate for hydroxy-catalysis bonding. But it will be necessary to measure the mechanical dissipation of these silicon to silicon bonds. It could prove to be difficult to develop carbon dioxide laser based techniques to weld silicon fibers to silicon blocks and benches and we should expect to do research in this area. Vertical isolation provided by low mechanical loss optimally shaped Silicon cantilever blades will require development effort and furthermore studies on the mechanical loss and strength of such blades.

Compatibility of the suspension design to the cryogenic cooling will require a great deal of attention. In addition, it will be necessary to ensure that the motions of the thermal shields do not induce NN. Extensive simulation and modeling of the full suspension, core optics, thermal shielding, optical baffle with a heat load from the absorbed laser power will be required before mechanical engineering can begin. Additional conductive cooling requirements beyond the $O(4\mathrm{W})$ radiative while challenging will likely be required. A demonstration of a cryogenic silicon suspension will be required but not necessarily at full scale. Although at some point a full scale test at LASTI is likely.

6.1.3 Suspensions for the Green Design

The suspension for large delay line mirrors will require special attention especially if they share an ISI with the core optics. The suspension point intefrometer (SPI) will require special attention because of its complicated mechanical dynamics, accommodation of the two optical paths in the aperture limited by the tube diameter and possible introduction of suspension thermal noise.

6.2 Seismic Isolation Systems

All three suspension designs are based on an Internal Seismic Isolation (ISI) system which can operate with a total payload equal to that of aLIGO. However, the size of the final stage core optic will be increased in all three cases to roughly 150 kg by redistributing

the mass between the 4 stages of the suspension and by reducing the ballast mass on the ISI. While modeling work will be required to determine for certain, it appears that we should be able to accomplished for all three quadruple suspension designs modifications to the existing ISI that will support the heavier suspensions. Reseach may be required to make more sensitive seismometers and displacement sensors possibly by modifying existing seismometers or building better displacement sensors for both designs to improve the active isolation of the ISI.

6.3 Newtonian Noise Subtraction

All three designs will require Newtonian Noise Subtraction with the Red Design requiring a factor of 5, and the Blue and Green Designs a factor of 30 suppression. This work is already underway as part of the risk reduction effort for aLIGO and Harms and Driggers are moving forward with Newtonian Noise study at the LIGO sites. One outcome of this work could be to decide whether or not Newtonian noise from the walls, ceiling and atmospheric sound noise from outside the buildings can be disregarded. If not it may be necesasary to study it for all three designs. Also the detailed understanding of correlations between ground motion around the test masses will inform the configuration of a seismic sensing array. In this study we aim to extend the research plan to include simulations for estimating the maximum possible subtraction with a given level of correlation and a given seismometer array. This work will inform all three designs. It will probably be necessary as part of the research into NN subtraction to make a 3D model of the geology around all of the observatory sites. The data collected from the measurements referred to in [Harms] will be very useful for this. A Monte-Carlo method could be used to compute a likely pressure/density wave spectrum within the rock that could give rise to the observed seismic spectrum at the surface. The model could be essential in determining the transfer function from density perturbations in the rock to acceleration measurements at the surface. Since we also in principle know the transfer function from density perturbations to the seismometer signals, we can estimate the maximum correlation between the seismometer signals and the NN as it appears in the gravitational wave channel. Finite-difference time-domain simulations may prove more useful than frequency domain calculations using spectra here. The Blue and Green Designs require a factor of 30 suppression. There could be a considerable amount of additional research and development required to obtain this additional factor of 6 suppression. It is also possible that the motions of the cryogenic system may produce additional NN.

[Harms] J. Harms, Newtonian noise research at the aLIGO sites, 2011.

[Driggers] refer J. Driggers “Newtonian noise subtraction” in PRD. [4]

6.4 Lasers

The laser design for the Red and Green designs on one hand and Blue designs on the other are very different and there is no common research and development for them.

6.4.1 Laser for the Red and Green Designs

The Red Design and the Green RDL Design are based on the aLIGO PSL, a Diode Laser Pumped injection lockes oscillator at 1064 nm. While the current Red design requires no more power than aLIGO the Green design will require about twice the laser power. The addition of a further stage of amplification should be straightforward for the Green design to achieve 250 watts.

6.4.2 Laser for the Blue Design

The Blue Design requires a 500-600 W laser operating at 1560 nm. While such a laser is not currently available there is considerable commercial and academic activity today focused on fiber lasers. The highest power (commercially available) linearly polarized, single mode 1560 nm laser currently available is a 100 W diode pumped Erbium fiber laser Newfern. We do not expect the output power of commercial single frequency lasers to continue to increase over the next several years. For a single frequency fiber laser there is likely to be a limit set by Brillion scattering at $\sim$200 W. Kilowatt class fiber lasers for machining applications are available today based on photonic crystal fibers but most are 1064 nm sources. The research necessary to push the technology in the direction we need seems feasible given the current world wide effort in fiber lasers and photonic crystals development. Moreover, LSC scientists have begun preliminary discussions with two commercial vendors and plan visits to those two over the next several months. These vendors have shown an interest in trying to combine these two technologies for both single frequency and high power operation. There is also considerable military research on 2 micron lasers at much higher power. The detection of high power 2 micron radiation woulod then become an issue.

6.5 Core Optics

For $\sim$150 kg silicon and silica core optics the technology for making the boules is already in hand. Grinding and polishing should also not be a big problem for either material. There should be no fundamental problems with the Ion Beam Figuring (IBF) of Silicon (as is now done with silica) to maintain micro roughness at the super polish level provided we remove no more than $\sim$100 nm of material in the refiguring process. The vendor figure metrology which is part of the figuring and polishing at the vendors will be more difficult. See the section on metrology below.

6.5.1 Core Optics for the Red and Green Designs

Large silica substrates while expensive are already available in the volume and form factor required for the Red design from the aLIGO core optics substrate supplier. Methods to characterize and potentially reduce fused silica surface loss, bonding loss and weld loss will need to be investigated and further demonstrated. Heraeus glass can currently pour 200 kg pots of the highest grade silica (Suprasil 3001). The cost for a single blank is, however, $\sim 10^6$ USD. The figure error and astigmatism requirements will require additional work for the larger spot sizes invisioned in these two designs.

6.5.2 Core Optics for the Blue Design

Silicon boules of 46 cm diameter are already being grown at semiconductor grade purity levels. There should be no problems in obtaining large enough substrates to accommodate up to 200 kg mirrors of the typical aspect ratio used in aLIGO.

The optical absorption of this grade of Silicon while low is not known to reach the level required for the Blue design. Also, silicon substrate absorption will have to be studied as a function of temperature. The CTE difference between silicon and the epitaxial coatings combined with annealing at 100 C and operating at 120 K could result in coating stress and birefringence. Moreover, we will need to investigate the optical homogeneity of these boules. The longer wavelength may provide an advantage because at the same figure error and microroughness the losses will be half as large as for aLIGO. Moreover the smaller sized beams will require stringent figure error control over a smaller area than the Red and Green designs. It should be noted that the Blue Design employs highest laser power (450W) of the 3 designs, despite cryogenic operation. Shortfall on coating absorption numbers can make this impossible.

6.6 Optical Metrology

Fizeau metrology interferometers of sufficient aperture already exist for substrates of the sizes currently discussed for both the Red, Green and the Blue designs. Metrology is probably doable with the larger substrates but the references spheres will be very expensive. It is not clear at this point if polishing vendors have the technology required to measure such a large reference surface. The current working aperture of the aLIGO metrology interferometer is 400 mm and stitching images together is difficult while maintaining the figure error measurement required. The biggest problems for both large silica and silicon core optics will be in requirements for an infrastructure that can handle these larger and heavy substrates. Moreover the measurements on these larger substrates will require substantial changes to the supporting or cradling structures used to hold the test masses in the interferometer. In addition, it will be necessary to redesign the whole Ergo arm approach to moving the optics. It may also be necessary to work out some sort of method to predict the change in the mirror surface when it is suspended in the GW detector and polish in the necessary surface figure error.

6.6.1 Optical Metrology for the Red and Green Designs

The metrology system upgrade to be able to handle the Red and Green Design silica substrates will be "relatively speaking" straightforward as discussed above.

6.6.2 Optical Metrology for the Blue Design

The metrology system for the Blue Design will require the change of metrology laser wavelength to 1560 nm and cameras that work at that wavelength. Finding a vendor who can figure and polish the reference spheres, has the in house metrology to work at 1560 nm and also has the surface measuring equipment to provide measured reference spheres could be

challenging.

6.7 Optical Coatings

There are three sources of loss related to the coatings including coating thickness nonunifrmity which leads to figure error, prompt scattering from microroughness and scattering from "inclusions" or "defects" in the coatings. These issues will be importabt for all three designs but the choice different materials will require parallel research efforts but they will probably use the same research approaches. The nonuniformity in coating thickness will probably not limit the performance of the squeezing cavities because the spots will be relatively small. However the microroughness and inclusion scatter could be a limitation to performance. This could require the investigation of coatings for operation at either 1064 nm or 1560 nm. These three effects limit cavity loss in the 4 km arms but the figure error due to coating nonuniformity will certainly limit the Red design and there is no information at all on the coating uniformity of large crystaline coatings so we should immediately begin studying this problem to determines the size of the effort required.

6.7.1 Optical Coatings for the Red Design

The Red design will require a modest improvement to the IBS coatings and a slightly larger spot size on the test masses. This will require improved figure error over a larger aperture which has been difficult in aLIGO. The improvement of the IBS coatings has a great deal of effort focussed on it and has had for some time. At this stage research should focus on improving both room temperature coatings for silica substrate and $1064nm$ wavelength. CSIRO IBS coating uniformity do not show any increase in figure error. The slightly larger spot on the core optics will require improved uniformity in the coating process but this will have to be done in collaboration with coating vendors. The use of a different kind of coating such as amorphous silicon could also be a route to improved coating thermal noise. A performance demonstration by making a direct thermal noise measurement may be required. There is also a large effort underway in the LSC to understand and improve the mechanical losses in IBS tantala and silica coatings and this work will have to continue.

6.7.2 Optical Coatings for the Blue Design

The Blue design will require the development of new generation of crystalline optical coatings and the LSC coating effort is now beginning to focus more on this research. In the longer term a collaborative effort must be undertaken with coating vendors to transfer that technology from the university to large commercial facilities to run in coating tanks which can coat 45 cm mirrors. The LSC should begin to reach out to the commercial houses to determine if there is any reason that these vendors would have for wanting to push this effort. Stress induced birefringence could introduce additional thermal noise and could depolarize the circulating beam in the arms leading to additional loss. The measurement of thermo-optical, thermo-mechanical, stress-optical, mechanical loss, scattered light, optical absorption (probably required at the 1 ppm level) , mechanical properties etc. will have to be measured at the temperatures we plan to use these coatings. This will be a large effort.

Ultimately a direct thermal noise measurement will be required of any crystaine coatings proposed for use in an interferometer. One area of important research will have to be the techniques to produce large area crystalline coating and the "attachment" of these coating on the mirror substrate. There is a growing effort underway in the LSC to measure mechanical losses in crystaline coatings and this effort will have to continue.

6.8 Coatings Thermal Noise Reduction

Both the Red and Green design will benefit from improved IBS Tantala and Silica based coatings including coating thickness uniformity and mechanical loss.

6.8.1 Coatings Thermal Noise Reduction for the Red Design

The Khalili cavity approach will require research on several fronts incuding the development of a deterministic control scheme, mode matching, the noises accociated with two additional optical cavities, accomodating the new optics into the vacuum system and an experimental demonstration at some scale of all of these.

The Red design alone could require work on a RWG mirror approach. These coatings would require research in almost all areas of coating development including: demonstration of the actual thermal noise level, RWGs with a multilayer coating, an understanding of the individual contributions of Brownian, thermoelastic and thermorefractive noise, development of more realistic noise estimates, measurement of mechanical quality factors of thin nanostructured tantala layers, direct measurement of coating thermal noise of a tantala RWG, increasing the reflectivity of tantala RWGs, Investigation of more tolerant grating designs, research into the RWG losses and absorption, characterization of scattered light, Improvement of each fabrication step in terms of line edge roughness and grating parameter homogeneity, fabrication of tantala gratings on 160 kg fused silica substrates, evaluation of different lithographic or imprint techniques with respect to the required substrate size and grating parameter homogeneity, evaluation of different etching techniques with respect to the required substrate size and grating parameter homogeneity.

6.8.2 Coatings Thermal Noise Reduction for the Blue Design

The Blue design would require work crystalling coatings and their transfer to silicon substrates. These coatings would require research in almost all areas of coating development including: demonstration of the actual thermal noise level, understanding of the individual contributions of Brownian, thermoelastic and thermorefractive noise, development of more realistic noise estimates, measurement of mechanical quality factors of both coating layers, direct measurement of coating thermal noise, research into losses and absorption, characterization of scattered light, Improvement of the coating transfer technique, fabrication of coatings of sufficicnt area and transfer to 160 kg fused silicon substrates.

6.9 Input Optics

6.10 Input Optics

All designs will have larger beams in the arms and so may require larger input beams thus requiring larger input optics. Also the Recycling optics may have to be made larger to be compatible with the larger beams in the arms.

6.10.1 Input Optics for the Red Design

No research on input optics for the Red design is expected beyond that discussed above.

6.10.2 Input Optics for the Green Design

The Green SPI Design requires significant upgrade of the input optics in order to accommodate two interferometers in a single vacuum manifold. It is not clear yet how to handle the beam at the vertex area. The high power interferometer of the SPI employs twice the power of the aLIGO laser. The requirements for the input optics should be revisitied.

6.10.3 Input Optics for the Blue Design

Every optic the beam passes through will have to be replaced. Also the higher input power may lead to the need for a thermal compensationb system for some of the critical input optics. This will probably nor require a additional research effort except for the Faraday isolator.

6.11 Thermal compensation

6.11.1 Thermal compensation for the Red Design

Since the stored power in the arms will be the same, there will be no upgrade for the themal compansation system for the arm cavities. Nevertheless, it is critical to employ TCS for the Khalili cavities to ensure the coupling of the beam to the Khalili cavities as designed. Also the upgrade of the TCS for the arm cavity may be necessary in the case of utilizing alternative beam shape. In each case, investigation of the requirements and detailed design will be required required. If RWG is needed then depending on the coating absorption the TCS requirements may need to be more diffiult to meet and research in this area may be needed.

6.11.2 Thermal compensation for the Blue Design

Thermal lensing in the Silicon mirror is expected to be at the same level as that of aLIGO. The cryogenic fused silica compensation plate at higher power would require additional research.

6.11.3 Thermal compensation for the Green Design

For the Green RDL Design, thermal effect of the large delay line mirrors will need to be be investigated. Since the Green SPI Design employs a high power laser with a smaller spot the evaluation of thermal lensing and its compensation will need to be be carried out.

6.12 Auxiliary Optics - SLC, TMS, OpLev, Initial alignment

Stray light control will need to be reevaluated for all designs becuse of the increased seisitivity. TMS will also need additional investigation because of the larger beams employed. aLIGO optical levers will be conserved for all designs and so no work will be needed. Initial alignment should be the same as for aLIGO.

6.12.1 Auxiliary Optics for the Red Design

If the IBS coating can be improved by a factor of 2 then no research on auxiliary optics for the Red design is expected. If Khalili cavities are required then

6.12.2 Auxiliary Optics for the Blue Design

High efficiency photodiodes at 1560nm will need to be explored. Acceptable maximum power level by such photodiodes have influence on the design of the sensing and control scheme. There should be less scattered light from the longer wavelength light but this advantage may be washed out buy the larger circulating power. A quantative assessment will be necessary. Arm Length Stabilization (ALS) system is employed in aLIGO in order to faclitate deterministic locking. This uses frequency doubled beams to control the arm lengths in terms of the main PSL beam. Since the silicon does not transmit 780nm light an alternative technique for ALS will have to be developed. A straightforward extention of ALS might be to use any phase locking technology between the main 1560nm beam and an auxiliary beam of a different wavelength. This could be implemented using a frequency comb technique or a heterodyne interferometry with pseudo-random modulation.

6.12.3 Auxiliary Optics for the Green Design

In the Green RDL Design there would not need to be any change here. Similarly to the input optics, the Green SPI Design involves great amount of complication for auxiliary optics. The practical arrangement should be explored.

6.13 Frequency Dependent Squeezing

All of the designs, except the high power Green SPI Design, employ frequency independent squeezing as a baseline. The Blue and Green RDL Design employs 10dB of squeezing while the Red and Green SPI use 20dB of squeezing. In any of these cases, most of the technical difficulties are related to optical losses and phase noise/rotation. Optical losses, such as scattering, absorption or mis-modematchin mix vacuum fluctuations with the squeezed

state. The main contributions to the loss budget are the output mode cleaner, Faraday isolators, modematching, and photodetector quantum efficiency and at low frequencies most imporantly losses are due to scattering in the filter cavity. Each of these elements need to be improved in order to be able to reduce the total loss budget down to approximately 15% which would allow an observed squeezing of 6dB. For 10dB or 20dB of squeezing a much more strict control of the losses is required. Phase noise and rotation, mainly due to the filter cavity, mix anti-squeezing with the squeezed state. Thus it is important to develop a locking scheme for the filter cavity to control the filter cavity length and alignment.

The filter cavity will probably require an extension of the vacuum system to accommodate this cavity. Thus once early filter cavity experiments have lead to experimentally informed designs, modifications of the vacuum system and the facility need to be addressed.

We will have to study the relative loss of optical systems based on different wavelengths. Moreover, research will have to be continued on developing a good error signal for controlling the squeezing ellipse angle for all three the designs.

6.14 Cryogenic Suspension for the Blue Desgn

Substantial research and engineering work will be required on the thermal engineering including any heat links (if conductive cooling is used) and radiative heat extraction (modeling indicated 3-10W but more work will be required). A demonstration (possible a prototype not to full size) will be required to demonstrate performance under a simulated heat load. The suspension performance will have to be demonstrated at low temperature. A very preliminary cryogenic design T1200093 exists. It is expected that a strong engineering team will be needed in this work. While 120K operation using radiative cooling is a novel idea much research and engineering design work will be required including careful attention to how the presence of compensation plate (at 122K) and the beam tube aperture (a black body at) only 10m distance effect performance. Supplemental conductive cooling may be required, placing a constraint on the fibers. Fiber heat conductivity can also be dependent on the material purity due to phonon scattering.

7 Conclusions

Through the mechanism of the Strawman design challenge, we have nearly 3 distinct designs with their various pros and cons. Very roughly speaking, all 3 designs have the same sensitivity.

None of the designs are yet solid; some kinds of unproven technology are invoked in order to make the sensitivity estimates made here. The aim is to continue development of these ideas to drive the R&D in the LSC and to eventually produce a conceptual design for the LIGO-III interferometers.

References

[1] Rana Adhikari, Guido Mueller, Norna Robertson, David McClelland, Yanbei Chen, Sam Waldman, Koji Arai, and Gregg Harry. LSC Instrument Science White Paper. Technical Report T1100309, LIGO, 2011.

[2] S. Hild, S. Chelkowski, A. Freise, J. Franc, N. Morgado, R. Flaminio, and R. DeSalvo. A xylophone configuration for a third-generation gravitational wave detector. *Class. Quantum Grav.*, 27:015003, 2009.

[3] S Hild, M Abernathy, F Acernese, P Amaro-Seoane, N Andersson, K Arun, F Barone, B Barr, M Barsuglia, M Beker, N Beveridge, S Birindelli, S Bose, L Bosi, S Braccini, C Bradaschia, T Bulik, E Calloni, G Cella, E Chassande Mottin, S Chelkowski, A Chincarini, J Clark, E Coccia, C Colacino, J Colas, A Cumming, L Cunningham, E Cuoco, S Danilishin, K Danzmann, R De Salvo, T Dent, R De Rosa, L Di Fiore, A Di Virgilio, M Doets, V Fafone, P Falferi, R Flaminio, J Franc, F Frasconi, A Freise, D Friedrich, P Fulda, J Gair, G Gemme, E Genin, A Gennai, A Giazotto, K Glampedakis, C Grf, M Granata, H Grote, G Guidi, A Gurkovsky, G Hammond, M Hannam, J Harms, D Heinert, M Hendry, I Heng, E Hennes, J Hough, S Husa, S Huttner, G Jones, F Khalili, K Kokeyama, K Kokkotas, B Krishnan, T G F Li, M Lorenzini, H Lck, E Majorana, I Mandel, V Mandic, M Mantovani, I Martin, C Michel, Y Minenkov, N Morgado, S Mosca, B Mours, H MllerEbhardt, P Murray, R Nawrodt, J Nelson, R Oshaughnessy, C D Ott, C Palomba, A Paoli, G Parguez, A Pasqualetti, R Passaquieti, D Passuello, L Pinard, W Plastino, R Poggiani, P Popolizio, M Prato, M Punturo, P Puppo, D Rabeling, P Rapagnani, J Read, T Regimbau, H Rehbein, S Reid, F Ricci, F Richard, A Rocchi, S Rowan, A Rdiger, L Santamara, B Sassolas, B Sathyaprakash, R Schnabel, C Schwarz, P Seidel, A Sintes, K Somiya, F Speirits, K Strain, S Strigin, P Sutton, S Tarabrin, A Thring, J van den Brand, M van Veggel, C van den Broeck, A Vecchio, J Veitch, F Vetrano, A Vicere, S Vyatchanin, B Willke, G Woan, and K Yamamoto. Sensitivity studies for third-generation gravitational wave observatories. *Classical and Quantum Gravity*, 28(9):094013, 2011.

[4] J. C. Driggers, J. Harms, and R. Adhikari. Newtonian noise subtraction. in prep., 2012.

[5] K G Lyon, G L Salinger, C A Swenson, and G K White. Linear thermal expansion measurements on silicon from 6 to 340 K. *Journal of Applied Physics*, 48(3):865–868, 1977.

[6] Rainer Weiss. Silicon mirror cooled to 120k. Technical Report T1200093-v1, LIGO, 2012.

[7] Garrett D. Cole, Simon Groblacher, Katharina Gugler, Sylvain Gigan, and Markus Aspelmeyer. Monocrystalline al[sub x]ga[sub 1 - x]as heterostructures for high-reflectivity high-q micromechanical resonators in the megahertz regime. *Applied Physics Letters*, 92(26):261108, 2008.

[8] N. Nakagawa, E. K. Gustafson, Peter T. Beyersdorf, and M. M. Fejer. Estimating the off resonance thermal noise in mirrors, fabry-perot interferometers, and delay lines: The half infinite mirror with uniform loss. *Phys. Rev. D*, 65:082002, Mar 2002.